The DOI for this manuscript is doi: 10.1175/2009JCLI3188.1

# The Physical Mechanisms by which the Leading Patterns of SST Variability Impact U.S. Precipitation

Hailan Wang[12], Siegfried Schubert[1], Max Suarez[1] and Randal Koster[1]

*1 Global Modeling and Assimilation Office, Science and Exploration Directorate, NASA GSFC, Greenbelt, Maryland*
*2 Goddard Earth Sciences and Technology Center, University of Maryland at Baltimore County, Baltimore, Maryland*



Submitted to the *Journal of Climate* for consideration in the *USCLIVAR drought working group Special Issue*

Revised in August 2009

ABSTRACT

This study uses the NASA NSIPP-1 AGCM to investigate the physical mechanisms by which the leading patterns of annual mean SST variability impact U.S. precipitation. The focus is on a cold Pacific pattern and a warm Atlantic pattern that exert significant drought conditions over the U.S. continent. The precipitation response to the cold Pacific is characterized by persistent deficits over the Great Plains that peak in summer with a secondary peak in spring, and weakly pluvial conditions in summer over the Southeast (SE) U.S. The precipitation response to the warm Atlantic is dominated by persistent deficits over the Great Plains with the maximum deficit occurring in late summer. The precipitation response to the warm Atlantic is overall similar to the response to the cold Pacific, with however considerably weaker amplitude.

An analysis of the atmospheric moisture budget combined with a stationary wave model diagnosis of the associated atmospheric circulation anomalies is conducted to investigate mechanisms of the precipitation responses. A key result is that while the cold Pacific and warm Atlantic are two spatially distinct SST patterns, they nevertheless produce similar diabatic heating anomalies over the Gulf of Mexico during warm season. In the case of the Atlantic forcing, the heating anomalies are a direct response to the SST anomalies, whereas in the case of Pacific forcing they are a secondary response to circulation anomalies forced from the tropical Pacific. The diabatic heating anomalies in both cases force an anomalous low-level cyclonic flow over the Gulf of Mexico that leads to reduced moisture transport into the central U.S. and increased moisture transport into the eastern U.S. The precipitation deficits over the Great Plains in both cases are greatly amplified by the strong soil moisture feedback in the NSIPP-1 AGCM. In contrast, the

response over the SE U.S. to the cold Pacific during spring is primarily associated with an upper tropospheric high anomaly over the southern U.S. that is remotely forced by tropical Pacific diabatic heating anomalies, leading to greatly reduced stationary moisture flux convergences and anomalous subsidence in that region. Moderately reduced evaporation and weakened transient moisture flux convergences play secondary roles. It is only during spring that these three terms are all negative and constructively contribute to the produce the maximum dry response in spring.

The above findings based on the NSIPP-1 AGCM are generally consistent with observations, as well as with four other AGCMs participating in the USCLIVAR project.

## 1. Introduction

It is known that recurring patterns of Sea Surface Temperature (SST) variability exert profound impacts on a number of regional climates throughout the world at inter-annual to decadal and longer time scales. For the United States (U.S.), the most important SST variations are those associated with El Niño-Southern Oscillation (ENSO), and at longer time scales, a decadal pan-Pacific pattern related to the Pacific Decadal Oscillation (PDO) (e.g. Zhang et al. 1997), and the Atlantic Multi-decadal Oscillation (AMO) (Enfield et al. 2001) in the north Atlantic. Past observational studies, both instrumental (e.g., McCabe et al 2004) and paleo-climatic (e.g., Seager et al 2007), and modeling work (e.g., Schubert et al 2004a) have suggested the importance of cold SST anomalies in the Pacific and warm SST anomalies in the Atlantic in accounting for past droughts and drought frequency over the U.S. In addition, a global linear trend pattern and SST variations in the Indian Ocean appear to be important.

The linkages between the regional SST variations and U.S. drought have been extensively investigated using General Circulation Models (GCMs) and available observations. The use of the GCM modeling approach has gained popularity because of the improving fidelity of models in simulating U.S. hydro-climate variability. Recent studies have shown that, when forced with the observed SST, the current generation of Atmospheric GCMs (AGCMs) is capable of reproducing the major U.S. droughts from the early twentieth century to the present (e.g., Schubert et al. 2004a; Seager et al. 2005). Atmospheric Model Inter-comparison Project (AMIP) type experiments (AGCMs forced with observed SSTs) have been used to investigate the causes of historical and recent U.S. droughts (e.g., Hoerling and Kumar 2003; Schubert et al. 2004b). In addition,

idealized AGCM experiments forced with fixed SST anomalies associated with the leading SST Empirical Orthogonal Functions (EOFs) have provided a useful framework for isolating and assessing the roles of the leading SST patterns of variability in forcing U.S. hydro-climate variations (e.g. Schubert et al. 2004a; Wang et al. 2009). However, the exact physical mechanisms by which the leading patterns of SST variability affect the U.S. hydro-climate in the GCMs, and the issue of model dependence of the results have not been sufficiently addressed. A systematic investigation of these mechanisms in AGCM experiments is necessary to improve our understanding of the model behavior in representing the linkage between SST and U.S. drought as well as the role of soil moisture.

The recent modeling efforts initiated by the United States contribution to the World Climate Research Programme's Climate Variability Study (USCLIVAR) drought working group (Schubert et al. 2009, this issue) provide an excellent opportunity to investigate the mechanisms through which the leading SST patterns affect the regional hydro-climate in the current generation of AGCMs, and to address the issue of the model dependence in representing the linkages between the leading SST patterns and U.S. drought. The participating AGCMs are the National Aeronautics and Space Administration (NASA) Seasonal-Interannual Prediction Project (NSIPP) version 1 AGCM at the Global Modeling and Assimilation Office (GMAO) (Bacmeister et al. 2000), the National Centers for Environmental Prediction (NCEP) Global Forecast System (GFS) (Campana and Caplan 2005), the National Center for Atmospheric Research (NCAR) Community Climate Model (CCM3) (Kiehl et al. 1998), the Geophysical Fluid Dynamics Laboratory (GFDL) AM2.1 (Delworth et al. 2006) and the

NCAR Community Atmosphere Model (CAM3.5) (Oleson et al. 2008; Stockli et al. 2008). The simulations include a series of idealized AGCM experiments using different AGCMs forced with SST anomaly patterns associated with the leading SST variability. The leading SST patterns are those of the leading SST EOFs of annual mean Hadley SST (Rayner et al. 2003) over 1901-2004, consisting of a globally warming trend pattern, a Pacific pattern, and an Atlantic pattern. These SST patterns respectively represent a global warming mode, a mixed decadal and ENSO variability in the Pacific, and an Atlantic multi-decadal variability pattern that resembles the AMO.

This study focuses on the results of the USCLIVAR simulations produced by the NASA NSIPP-1 AGCM. In particular, we perform an in-depth investigation of the physical and dynamical mechanisms through which the cold Pacific and warm Atlantic SST patterns, the two major U.S. drought inducing SST patterns, influence the U.S. precipitation in the NSIPP-1 model. We focus on the NSIPP-1 AGCM experiments because we have available to us a complete set of model output, including daily data and three-dimensional (3-D) monthly diabatic heating fields, that are necessary for assessing budgets and various dynamical forcing fields. We do, however, address the issue of model dependence by comparing with other AGCMs participating in the drought working group modeling efforts those results that are available to us from a common set of model output fields. In addition, to the extent possible in an idealized setting, we compare the results with observations.

This paper is organized as follows. Section 2 describes the data and methods. Section 3 examines the regional and seasonal characteristics of the precipitation responses of the NSIPP-1 AGCM to the three leading SST patterns. Section 4

investigates the physical mechanisms by which the cold Pacific and warm Atlantic SST patterns affect the U.S. precipitation in the simulations. That section also addresses the issues of model dependence, the significance of seasonal variations of SST anomalies associated with the leading SST patterns, and the comparison with observations. The summary and conclusions are given in Section 5.

## 2. Data and methods

### *a. AGCM experiments and observational data sets*

In the idealized AGCM experiments initiated by the USCLIVAR drought working group, the SST anomaly patterns are fixed and superimposed on the monthly varying SST climatology (1901-2004). The amplitudes for the Pacific and Atlantic SST patterns correspond to 2 standard deviations of their Principal Components (PCs) so as to strongly force the models to obtain robust model responses, whereas the amplitude for the Trend pattern is 1 standard deviation. The simulations with the NSIPP AGCM forced with the Pacific and Atlantic SST anomaly patterns are each 99 years long, and the experiments for the Trend pattern are 50 years long. The simulations with the NCAR CCM3, GFDL AM2.1 and NCAR CAM3.5 are each about 50 years long, and about 35 years long for the NCEP GFS model. The model responses to the leading Pacific and Atlantic patterns in the NSIPP-1 AGCM are obtained as the mean differences between the control run and the anomaly runs averaged over the last 80 years, whereas those for the Trend pattern with the NSIPP AGCM and all SST patterns with the other models are obtained by averaging over the last 50 years (35 years for the NCEP GFS). More details of the leading SST patterns, the AGCM experiment design, the participating AGCMs and an overview of the model inter-comparison results can be found in Schubert et al. (2009, this issue). Details

of the NSIPP-1 model formulation and its climate are described in Bacmeister et al. (2000). The seasonal predictability of the model is described in Pegion et al. (2000) for boreal winter, and in Schubert et al. (2002) for boreal summer.

In parallel to the primary idealized AGCM experiments already described, a series of auxiliary experiments were performed in which we disable the soil moisture feedback by prescribing soil moisture to its (geographically-varying) climatological seasonal cycle. In these simulations, soil moisture is not allowed to increase in response to a given precipitation event, and thus subsequent evaporation is also not allowed to increase and thereby act to further enhance the precipitation. The comparison between these two series of experiments shows the impact of land-atmosphere feedback processes on the precipitation responses over the U.S.

To assess the impact of month-to-month variations of SST anomalies associated with the leading patterns (the idealized anomalies are fixed in time) as well as to facilitate the comparison with observations, we also examine an ensemble of 14 AMIP simulations made with the same NSIPP-1 AGCM covering the period 1902-2004. Details of these AMIP runs are described in Schubert et al. (2004a). The observational data used for comparison are the monthly Hadley Centre Global Sea Ice and Sea Surface Temperature (HadISST) (Rayner et al. 2003) over the period 1901-2004, monthly mean precipitation over the period 1948-2004 computed from a retrospective analysis of daily station precipitation over the United States and Mexico (US-MEX) provided by the NCEP Climate Prediction Center (CPC)[1], and monthly zonal and meridional wind fields from the NCEP/NCAR Reanalysis (Kalnay et al. 1996) for the period 1948-2004.

[1] More information about the data are available at http://www.cpc.ncep.noaa.gov/products/precip/realtime/retro.shtml.

*b. Methods*

To facilitate the investigation of the mechanisms by which the leading SST patterns affect the U.S. precipitation, atmospheric moisture budget analysis and stationary wave modeling diagnosis are performed.

The atmospheric moisture budget analysis reveals how precipitation responses over the U.S. are balanced by evaporation responses and changes in atmospheric transient and stationary moisture flux convergences, a technique that has been widely used in the past (e.g., Roads et al. 2002). The budget analysis is based on the vertical integral of the equation for atmospheric water vapor in pressure coordinates:

$$\frac{1}{g}\int_{P_{sfc}}^{P_{top}}\frac{\partial q}{\partial t}dp+\nabla\bullet\frac{1}{g}\int_{P_{sfc}}^{P_{top}}qVdp=E-P \qquad (2.1)$$

where q is specific humidity, V is the three-dimensional wind in pressure coordinates, E evaporation, and P precipitation. Each variable ( $A$ ) is separated into its mean ( $\overline{A}$ ), i.e., the climatology of the control run, and deviation from the mean ( $A'$ ), i.e., the mean difference between an anomaly run and the control run. Equation (2.1) then becomes:

$$P'=E'+qconv'_{tran}+qconv'_{stat}-\frac{1}{g}\int_{P_{sfc}}^{P_{top}}\frac{\partial q'}{\partial t}dp \qquad (2.2)$$

where $qconv'_{tran}=-\nabla_h\bullet\frac{1}{g}\int_{P_{sfc}}^{P_{top}}(\overline{q_{anom}''V_{hanom}''}-\overline{q_{ctrl}''V_{hctrl}''})dp$

$$qconv'_{stat}=qconv'_{statV}+qconv'_{statQ}$$

$$qconv'_{statV}=-\nabla_h\bullet\frac{1}{g}\int_{P_{sfc}}^{P_{top}}(\bar{q}V_h')dp\ ,\ qconv'_{statQ}=-\nabla_h\bullet\frac{1}{g}\int_{P_{sfc}}^{P_{top}}(q'\overline{V_h})dp$$

In the above equations, $\nabla_h$ denotes horizontal divergence, $V_h$ the horizontal winds, $''$ indicates transient deviation from monthly mean, the subscripts $anom$ and $ctrl$ refer to an anomaly run and the control run respectively. Thus, the change in precipitation ($P'$) is balanced by the change in evaporation ($E'$), the vertical integral of the change in transient moisture flux convergences ($qconv'_{tran}$), the vertical integral of the change in stationary moisture flux convergences ($qconv'_{stat}$) - the sum of the contribution from change in mean atmospheric circulation ($qconv'_{statV}$) and that from change in mean atmospheric water vapor ($qconv'_{statQ}$), and the vertical integral of the change in atmospheric water vapor ($-\frac{1}{g}\int_{P_{sfc}}^{P_{top}} \frac{\partial q'}{\partial t} dp$). The last term ($-\frac{1}{g}\int_{P_{sfc}}^{P_{top}} \frac{\partial q'}{\partial t} dp$) is at least one order of magnitude smaller than the rest terms and can be ignored.

In computing the budgets for the Pacific and Atlantic patterns, the vertical integrals of the transient and stationary moisture flux convergences terms are pressure-weighted, following Roads et al. (2002). The transient term is obtained as deviation from monthly mean and thus is of submonthly timescale. Note that the atmospheric moisture budget analysis for the NSIPP-1 AGCM is not strictly closed (Nigam and Ruiz-Barradas 2006) due to model output limitations. The wind and specific humidity fields are given at pressure levels instead of the original model coordinates, and thus contain errors associated with the spatial interpolation between these coordinates. Furthermore, the model wind fields are at spatial grids different from the water vapor fields, potentially introducing additional errors to the moisture budget. However, our experience is that any such errors do not affect the basic conclusions we draw from the budgets.

Since the leading SST patterns affect the U.S. climate by forcing changes in atmospheric circulation over the U.S., a stationary wave model is used to diagnose the maintenance mechanisms of atmospheric circulation changes. The stationary wave model is essentially a dry dynamical core of another AGCM (Ting and Yu 1998). It is based on the 3-D primitive equations in σ coordinates, and is time-dependent and nonlinear. The model-generated transient disturbances are suppressed by strong damping. The model has rhomboidal wavenumber-30 truncation in the horizontal and 14 unevenly spaced σ levels in the vertical (R30L14). The stationary wave model has been shown to be a valuable tool to diagnose the maintenance of both climatological and anomalous atmospheric circulation by evaluating the relative roles of stationary wave forcings over specific regions (Ting et al. 2001; Held et al. 2002; Lau et al. 2004). More details of the stationary wave model can be found in Ting and Yu (1998).

In the stationary wave modeling experiments performed in this study, the background state is the climatological 3-D seasonal mean flow of the control run. The stationary wave forcings for the anomalous atmospheric circulation include the 3-D anomalous diabatic heating and transient flux convergences that are obtained as the mean differences between an anomaly run and the control run. The diabatic heating is taken from the model output directly and linearly interpolated to a resolution of R30L14 to be consistent with the stationary wave model. Since the NSIPP-1 AGCM model output does not include a few terms necessary for the calculation of the transient forcing as a residual, the transient forcing is obtained by explicitly computing the major terms in the 3-D primitive equations in pressure coordinates, and then linearly interpolated onto the R30L14 resolution. Such estimates of the transient forcing are generally weaker than

those derived as a residual, and contain errors that lead to differences between the stationary wave model simulation and the stationary wave anomalies in the AGCM simulation especially in cold seasons when transients are more important. In addition, the anomalous stationary wave forcings associated with the leading SST patterns are not strong enough to lead to significant stationary nonlinearity; the stationary wave modeling solutions are largely linear.

**3. Seasonal mean precipitation responses to the leading SST patterns**

Figure 1 shows the seasonal mean precipitation responses over the U.S. to the leading SST patterns in the NSIPP-1 idealized runs. The response to the cold Trend pattern is not included due to its weak response over the U.S. Figure 1 shows that, over the U.S., a warm Pacific and cold Atlantic lead to general pluvial conditions, whereas a cold Pacific, warm Atlantic and warm Trend lead to general drought conditions. The precipitation responses to the Pacific pattern are considerably stronger than those to the Atlantic and Trend patterns. In general sense, for both the Pacific and Atlantic SST forcing patterns, changing the sign of the forcing patterns essentially acts to change the sign of the precipitation responses over the U.S.

The precipitation response to the cold Pacific (Fig.1b) shows interesting seasonal and regional variations. During winter, the cold Pacific SST forces a strong and significant precipitation reduction along the southern and southeastern coasts of the U.S., and a precipitation increase over the northwestern U.S. During spring, while there is a precipitation increase over the northwestern U.S., the majority of U.S. experiences a precipitation deficit, with the largest precipitation reduction centered on the southern Great Plains and the South East (SE) U.S. The summertime precipitation response is

characterized by a strong precipitation reduction over the Great Plains with precipitation increases to the west and east. In fall, while the precipitation deficit over the central U.S. weakens, much of the country again experiences widespread precipitation deficits, with the maximum deficit centered over the southwestern U.S. These deficits are accompanied by moderate but significant precipitation increases along the northwestern and southeastern U.S. coasts. The seasonal mean precipitation response to the warm Pacific (Fig.1a) is generally opposite to that of the cold Pacific (Fig.1b), with the main differences appearing over the northwestern U.S. during fall and winter when the amplitude of precipitation decreases in Fig.1a are considerably stronger and significant. While the Pacific pattern in the idealized runs is fixed throughout the seasonal cycle, the model results (Fig.s 1a, 1b) are to a large extent consistent with past observational studies of the impacts of ENSO and PDO SST anomalies over the U.S. during winter (Ropelewski and Halpert, 1986; Higgins et al. 2000) and summer (Ting and Wang 1997; Barlow et al. 2001).

The seasonal mean precipitation response to the warm Atlantic (Fig.1c) is to some extent similar to the response to the cold Pacific, but with generally weaker amplitudes, especially in spring. The U.S. wintertime precipitation response to the warm Atlantic exhibits a significant wet response over the northwest and dry responses along the southern and southeastern coasts. In spring, the overall response is rather weak. The precipitation deficit over the central U.S. increases in summer, together with a precipitation surplus to the east. During fall, the majority of the U.S. is covered with significant precipitation deficits centered over the southwestern U.S. Overall the precipitation response to a warm Atlantic is dominated by the dry response over the

central U.S. that peaks in summer. The warm season precipitation response to the warm Atlantic pattern in Fig.1c is consistent with the observed effect of AMO in its warm phase over the U.S. (Enfield et al 2001). The responses to the cold Atlantic (Fig. 1d) are generally opposite to the responses to the warm Atlantic (Fig.1c).

The responses to the warm Trend pattern (Fig.1e) show a significant precipitation increase over the northwestern U.S. in winter and spring, and a notable dry response over the central U.S. that persists from spring to fall and peaks in summer.

Since the precipitation responses to the leading SST patterns are mostly over the Great Plains and the SE U.S., we further examine the seasonality of the precipitation responses averaged over these two regions. Over the Great Plains (Fig.2a), the warm Pacific and cold Atlantic SST patterns force persistent pluvial conditions that are rather weak in winter and become the strongest in late summer. In contrast, the cold Pacific, warm Atlantic and warm Trend SST force persistent drought conditions with the response to cold Pacific peaking in summer, and the responses to the warm Atlantic and warm Trend peaking in late summer. The responses to the Pacific patterns are much stronger than the other two patterns. The amplitudes of the precipitation responses to the Pacific patterns are at least two (four) times as strong as those of the Atlantic (Trend) patterns during late summer when the latter responses are the strongest.

Over the SE U.S. (Fig.2b), the response to the cold Pacific SST is characterized by a distinct contrast between a strong dry response in winter and spring and a moderate wet response in summer and early fall. The response shows a distinct maximum precipitation reduction in spring, a rapid recovery in early summer, a moderate precipitation increase in late summer and early fall, a return to near normal conditions in

fall, and a moderate precipitation deficit in winter. The response to warm Pacific SST is generally opposite to that to the cold Pacific, with the amplitudes of dry response during late summer and early fall considerably stronger than those of pluvial response. Such a seasonality of the precipitation response over the SE U.S. to the Pacific SST pattern is consistent with observations (Mo and Schemm 2008) in that cold (warm) ENSO events are associated with positive (negative) precipitation anomalies over the SE U.S. in winter but negative (positive) anomalies in summer. The precipitation responses to the warm (cold) Atlantic and warm Trend patterns show a wet (dry) response during summer and early fall and a dry (wet) response during the rest of the seasons, though these responses are generally weaker than the responses to the Pacific forcing.

In the rest of this paper, we will focus on those SST anomalies that produce the largest and/or most extensive precipitation deficits over the U.S., namely the cold Pacific and warm Atlantic patterns.

## 4. Mechanisms linking SST anomalies to U.S. precipitation deficits

Before looking in detail at the physical mechanisms that link the remote SST anomalies to changes in the U.S. hydroclimate, we take a brief look at the annual cycle of the area-averaged moisture budget terms for the Cold Pacific (SE and Great Plains) and warm Atlantic forcing (Great Plains). This should allow us to further focus our analysis on those key seasons when the SSTs have the greatest impacts.

### *4.1 The annual cycle of the atmospheric moisture budget*

Figure 3a shows that the peak precipitation deficit over the SE U.S. in MAM is mainly explained by the reductions in stationary moisture flux convergences over the southern U.S., with reduced evaporation playing a secondary role. The large precipitation

deficit in DJF, however, is mainly explained by the weakened transient moisture flux convergences. During winter, the model is well consistent with observations in that the cold Pacific forces an upper high anomaly over south and east U.S. that significantly alters the zonal flow over the U.S., weakens storm tracks over the SE U.S. and leads to dry condition there (not shown). The transients are rather weak in the rest of seasons. The stationary moisture flux convergences contribute to precipitation increases in winter and moderate increase in summer, but act to reduce precipitation in MAM - the season of maximum precipitation deficit in this region. The evaporation shows weak reductions from winter to early summer and weak increase in the rest of the seasons.

Over the Great Plains, the precipitation reduction in response to the cold Pacific (Fig.3b) occurs throughout the seasonal cycle with the peak in summer. During the warm season, the precipitation reduction is mainly explained by reduced evaporation, with the reduced stationary moisture flux convergence playing a secondary role. The contribution by changes in atmospheric stationary moisture convergence due to changes in atmospheric circulation and that due to changes in atmospheric moisture generally cancel each other, with the former considerably overwhelming the latter. The contribution by transients is rather minimal throughout the seasonal cycle. The relative roles of individual terms in balancing the precipitation response over the Great Plains to the warm Atlantic (Fig.3c) are generally similar to those for the cold Pacific, with however smaller amplitudes and the peak appearing in late summer. We will return to the similarity of these two responses in Section 4.4.

We next focus on those seasons for which the impacts are the largest. In particular, we perform an in-depth investigation of the physical mechanisms by which a

cold Pacific leads to precipitation deficits over the SE U.S. in March-May (MAM) and the Great Plains in June-August (JJA), as well as the mechanisms by which a warm Atlantic results in precipitation deficits over the Great Plains in July-September (JAS).

*4.2 A cold Pacific and precipitation deficits in MAM*

Figure 4 shows spatial maps of the various components of the atmospheric moisture budget for the precipitation responses to the cold Pacific in MAM for the standard run (Fig.4a) and the auxiliary run in which the soil moisture feedback is turned off (Fig.4b). As discussed below, Fig.4a and Fig.4b suggest that the precipitation deficit over the Great Plains is primarily explained by a local reduction in evaporation, with some contribution from changes in stationary moisture fluxes. Over the SE U.S., however, the precipitation deficit is mostly the result of greatly reduced stationary moisture flux convergence associated with a strong anticyclonic anomaly over the southern U.S. Such a circulation anomaly induces strong subsidence over the southern U.S. (Fig.4a) and is likely to facilitate the drought conditions there (Namias 1983). Meanwhile, the westerly and northwesterly winds at the north flank of the high anomaly result in weakened storm track along the southeastern U.S. and enhanced storm track further north (not shown). The associated changes in transient moisture flux convergences contribute to a moderate precipitation reduction along the southern coast of the U.S., and precipitation increase over the northern portion of the eastern U.S. The contribution to the changes in atmospheric stationary moisture convergence from changes in atmospheric moisture results in a precipitation increase over the SE U.S. and offsets the precipitation deficit there.

By design, the evaporation responses over the Great Plains and the SE U.S. essentially disappear when the soil moisture feedback is turned off. In effect, the only difference between the sets of runs examined in Fig.4a and Fig.4b is the lack of soil moisture feedback in the latter set and thus an inability of the land surface to amplify precipitation anomalies through this feedback – low precipitation cannot lead to reduced evaporation and thus to a reduced source of moisture for subsequent precipitation. The fact that the cold Pacific pattern reduces precipitation more in Fig. 4a than in Fig. 4b therefore suggests strongly that soil moisture feedback does indeed amplify the SST-induced anomaly. Soil moisture feedback, however, is not as important over the SE U.S., in agreement with previous results (Koster et al. 2000). The distributions of transient and stationary moisture flux convergences are essentially unaffected by the absence of the land-surface feedback. The precipitation change over the SE U.S. is mainly explained by changes in atmospheric circulation.

One caveat about soil moisture feedback is appropriate here. The NSIPP-1 model is known from a number of studies (e.g., Koster et al. 2003) to overestimate the feedback present in nature, as inferred indirectly from observations. Nevertheless, the observations-based inferences do show that feedback in nature generally occurs in the areas highlighted by the model, if at reduced levels (Koster et al. 2003; Koster and Suarez 2004; Koster et al. 2006b).

Given the prominent role of the anomalous high over the southern U.S. for the dry response in the SE U.S. as suggested by the lowest panels in Fig.4, we investigate its maintenance using a stationary wave model. An inspection of the 3-D structure of the high anomaly (not shown) indicates that it has a barotropic structure and that it has the

maximum amplitude in the upper troposphere, suggesting that the atmospheric circulation anomaly is remotely forced. In the following we use the stationary wave modeling approach to diagnose the MAM upper tropospheric circulation response to the cold Pacific.

Figure 5a shows that, in response to the prescribed cold Pacific pattern, there is a strong diabatic cooling response along the central and eastern tropical Pacific, straddled by diabatic heating anomalies to the north and south. Over North America, there is diabatic cooling over the Great Plains and SE U.S., associated with the wide spread precipitation deficits shown in Fig.1b. Over the Pacific-North-American (PNA) region, the upper tropospheric stationary wave response is characterized by a wave train emanating from the central and eastern tropical Pacific. The circulation response over the U.S. and surrounding regions features an anomalous high centered over the southwest U.S., the key feature of interest, as well as an anomalous low to the north.

The stationary wave model simulation forced with the total stationary wave forcing anomalies (Fig.5b), i.e., the sum of diabatic heating anomalies and transient flux convergences anomalies, is in good agreement with the AGCM simulations (Fig.5a) over the PNA region. The agreement west of the dateline is not as good, and may be due to the inaccuracy in the computed transient forcing as well as errors introduced when performing spatial interpolation of stationary wave forcings from the NSIPP model grids to the R30L14 resolution. The generally good agreement, especially over the PNA region, suggests that we can use the stationary wave model to further diagnose the relative roles of regional diabatic heating and transients in forcing the high anomaly over the southern U.S. The comparisons between Fig.s 5b-d show that the diabatic heating

anomaly plays a prominent role. It alone forces a wave train that emanates from the tropical Pacific across the North America, producing an anomalous high over the southern U.S. and a northwest-southeast tilted low further north (Fig.5c). An additional stationary wave modeling experiment forced with the diabatic heating anomaly in the Pacific only (not shown) shows that the response in Fig.5c is mostly excited by diabatic heating anomaly in the tropical Pacific. While the transients contribute to only a weak high over the central and eastern U.S. (Fig.5d), they act to shift the diabatically-forced high and low responses over the U.S. further eastward, closer to the locations in the AGCM simulations. Additional stationary wave experiments were done to assess the sensitivity of the results to the heating and the basic state. In particular, runs forced with mixed combinations of the seasonal 3-D background flow and seasonal diabatic heating anomaly (Fig.s 5e-f) show that the aforementioned stationary wave response over the PNA region in MAM is largely controlled by the 3-D climatological springtime background flow, with the seasonal changes in diabatic heating playing a secondary role. For example, if the MAM tropical Pacific heating anomalies are imposed upon the DJF mean background flow, the path of the Rossby wave propagation is altered with the PNA region dominated by northwest to southeast oriented wavetrain that results in a low anomaly over much of the U.S. (Fig.5e). By comparison, the response to the DJF tropical Pacific heating anomalies imposed on the MAM mean flow (Fig.5f) shows the correct basic wave structure over the PNA region (cf. Fig. 5c), although the center of the key high anomaly over the U.S. is displaced well to the south.

The above analysis suggests that the MAM precipitation deficits that develop in the Great Plains in response to the cold Pacific are initiated by the anomalous high and

associated subsidence that develops in that region as part of an upper wave response to the Pacific SST forcing. The subsidence leads to a precipitation reduction which is further amplified by local land-atmosphere feedback processes, and largely balanced by deficits in evaporation. In contrast, the strong precipitation reduction over the SE U.S. is mostly due to a reduction in the stationary moisture flux convergences as well as the subsidence induced by the high anomaly that extends across the SE U.S. The soil moisture feedbacks and reduced transient moisture flux convergence in this region play a secondary role.

*4.3 A cold Pacific and precipitation deficits in JJA*

Figure 6 shows components of the atmospheric moisture budget for the AGCM response to the cold Pacific pattern during JJA in both the standard run (Fig.6a) and the auxiliary run that has the soil moisture feedback turned off (Fig.6b). The comparison between the panels in Fig.6a shows that the precipitation deficit in the central U.S. is largely balanced by an evaporation deficit and reduced stationary moisture convergences due to atmospheric circulation changes, whereas the precipitation increases over the west and east U.S. are mainly balanced by the latter. The low-level atmospheric circulation changes are characterized by an anomalous low over the Gulf of Mexico that acts to weaken the Great Plains Low Level Jet (LLJ) and thus reduces the low-level atmospheric moisture transport from the Gulf of Mexico to the central U.S. In contrast, the northeastern flank of the low produces a precipitation increase over the eastern U.S. by converging moisture that enters the U.S. from the Atlantic. This also explains the moderate precipitation increase over the SE U.S. during summer (Fig.2b).

Figure 6a and Fig. 6b together suggest that soil moisture feedback processes in JJA greatly amplify the SST-induced precipitation reduction over the central U.S. even

more than they do in MAM, consistent with the idea that evaporation rates, and thus their impacts on the atmosphere, should be the strongest during summer. In the absence of land-atmosphere feedback, the amplitude of precipitation deficit over the central U.S. is weakened by more than 50% (Fig.6b).

We next turn to the maintenance of the JJA atmospheric circulation anomalies, in particular the low-level cyclonic anomaly over the Gulf of Mexico that appears to be the key to the dry response over the central U.S. (Fig.6). Figure 7a shows that the response to the cold Pacific SST pattern consists of strong cooling anomalies over the central and eastern tropical Pacific with heating anomalies to the west and south, and strong localized heating anomalies over the Gulf of Mexico with moderate cooling anomalies to its west and north in the U.S. The stationary wave response in the lower troposphere is characterized by a strong and localized cyclonic response over the Gulf of Mexico, the key feature of interest here, a cyclonic response over South America, and a pair of anticyclones straddling the equator in the western tropical Pacific. The strong similarity between the stationary wave model response to the total anomalous stationary wave forcing (Fig.7b) and the AGCM simulation (Fig.7a) suggests that the stationary wave model can be used to diagnose the AGCM response in summer. The comparison between Fig.7b and 7c indicates that it is the change in diabatic heating (Fig.7c) that accounts for the overall circulation anomaly; the anomaly in transients (not shown) plays a negligible role. We next examine the relative contributions of the diabatic heating anomalies in the remote Pacific and the local U.S. and Gulf of Mexico in maintaining the low-level cyclonic anomaly over the Gulf of Mexico. The comparison (Fig.s7c-f) clearly shows the dominant contribution by the local anomalous diabatic heating over the Gulf of Mexico

and the cooling anomaly over the central U.S., whereas the diabatic heating anomaly in the remote tropical Pacific plays a secondary role. The Gulf of Mexico heating anomaly forces a distinct low that centers over the Gulf of Mexico (Fig.7f), whereas the diabatic heating anomaly in the Pacific contributes to a rather extensive yet weak low anomaly over the entire North Atlantic and southeastern North America (Fig.7e).

Clearly, the aforementioned anomalies of atmospheric circulation and diabatic heating over the Gulf of Mexico and the central U.S. must originate from the Pacific SST forcing. Our analysis suggests that the impact of the strong diabatic cooling in the central tropical Pacific induces local subsidence and, via its impact on the Walker circulation, anomalous ascent over the tropical Atlantic. In the NSIPP-1 model, the anomalous ascendance leads to a strong diabatic heating anomaly over the Gulf of Mexico which excites a strong anomalous low-level low in that region (Fig.7f). The strong low-level cyclonic flow anomaly in turn weakens the Great Plains LLJ and reduces the moisture transport from the Gulf of Mexico to the continental U.S., leading to a drying (cooling) over the central U.S. and increased precipitation (heating) over the Gulf of Mexico. Meanwhile, the easterly anomaly on the north flank of the low-level cyclonic flow leads to increased precipitation over the eastern U.S. by converging moisture from the Atlantic. The strong soil moisture feedback over the central U.S. in the NSIPP model greatly enhances the SST-forced precipitation responses over the Great Plains. The anomalous diabatic heating and cooling anomalies over the Gulf of Mexico and the U.S. in turn excite changes in atmospheric circulations that further reinforce and strengthen themselves via weakened northward moisture transport, closing a positive feedback loop.

*4.4 A warm Atlantic and precipitation deficits in JAS*

Figure 8a shows the terms of the atmospheric moisture budget for the AGCM response to the warm Atlantic in JAS. The distributions of individual terms are remarkably similar to those for the cold Pacific (Fig.6a), but with somewhat weaker amplitude. The budget for the auxiliary run with soil moisture feedback disabled (Fig.8b) is overall similar to that for the cold Pacific in Fig.6b as well. The precipitation response to the warm Atlantic shows a strong drying over the central U.S. and a significant precipitation surplus over the eastern U.S. The precipitation decrease over the central U.S. is related to reduced stationary flux convergence associated with anomalous cyclonic flow over the Gulf of Mexico (Fig.8a), and is greatly amplified by the soil moisture feedback, as implied from the auxiliary run (Fig.8b). The precipitation increase over the eastern U.S. is mostly balanced by an increase in stationary flux convergence. The transients play a supporting role over both the central and eastern U.S., whereas the changes in water vapor convergence due to changes in water vapor tend to be of opposite sign.

In order to better understand why the moisture budget over the U.S. for the warm Atlantic is similar to that for the cold Pacific, we compare the maintenance of their circulation anomalies. Figure 9a shows that in response to the prescribed warm Atlantic SST anomaly, there is a strong and zonally elongated diabatic heating anomaly spanning from the Gulf of Mexico eastward to the west coast of Africa at about 12°N, with the maximum centered over the Gulf of Mexico. To its west is diabatic cooling that extends over Mexico and oceanic regions to the south. Associated with the anomalous ascent excited by the tropical Atlantic heating, there is also a band of moderate diabatic cooling

in the Northern Hemisphere (NH) subtropical Pacific. The summertime diabatic heating response to the warm Atlantic (Fig.9a) is broadly similar to that of the cold Pacific (Fig.7a) in the NH, with however the heating anomaly over the NH tropical Atlantic considerably stronger and the cooling and heating anomalies in the Pacific considerably weaker in the case of the Atlantic forcing. Similar to Fig.7, the stationary wave modeling results for the warm Atlantic show a good simulation of the AGCM results, and again highlight the dominant role of diabatic heating anomalies over the Gulf of Mexico in maintaining the low-level cyclonic flow there. Therefore, although the cold Pacific and warm Atlantic are two distinctly different SST patterns, they lead to similar diabatic heating and atmospheric circulation responses over the Gulf of Mexico. In the case of the Atlantic forcing, these responses are largely local responses to the prescribed Atlantic SST anomalies, while for the Pacific forcing, these are secondary responses to the Pacific SST anomalies via the forced changes in Walker circulation.

*4.5 Comparisons with other models and observations*

In this section we take advantage of the availability of selected results from other AGCMs that participated in the drought working group effort (see Section 1), and assess the model dependence of the responses to the idealized SST patterns for the seasons of relevance here. Figure 10 shows that there is generally good agreement between the NSIPP-1 and the four-model ensemble mean of the NCEP GFS, the NCAR CCM3, the NCAR CAM3.5 and the GFDL AM2.1. Such agreement is especially close for the MAM response to the cold Pacific pattern. Similar to the NSIPP idealized runs (left panels), the four-model ensemble mean (right panels) shows dry responses over the U.S. in MAM and JJA for the cold Pacific and in JAS for the warm Atlantic. The wavetrain pattern over

the PNA region in MAM response to the cold Pacific, the pair of cyclones over intra-America and the tropical Atlantic as well as the pair of anticyclones over the central tropical Pacific in the warm season responses to the cold Pacific and warm Atlantic are all clearly evident in the four-model ensemble mean. The differences between the NSIPP-1 and the four-model ensemble mean mainly appear in the warm season responses. The amplitudes of the model ensemble mean (Fig.s 10d, f) are generally weaker, partly due to the averaging over the four models. In addition, the NSIPP-1 model tends to place the strongest precipitation and low-level circulation responses over the Gulf of Mexico (Fig.s10c, e), whereas the four-model ensemble mean (Fig.s10d, f) has the strongest precipitation responses over the NH eastern tropical Pacific and the Caribbean regions; the low-level cyclonic anomalies over the Gulf of Mexico (Fig.s 10d,f) are weaker and less localized. Despite these differences in regional details, the overall good agreement between the NSIPP-1 simulations and the four-model ensemble mean suggests that our findings based on the NSIPP-1 runs, to a large extent, do not depend on the particular model we use. The warm season precipitation and low-level atmospheric circulation responses to the warm Atlantic in Fig. 10 are also in good agreement with those in Sutton et al (2005).

We next make a limited comparison with observations. Here we turn to an ensemble of fourteen AMIP-style simulations made with the NSIPP-1 model for the period 1902-2004. The ensemble mean of the atmospheric circulation and precipitation fields from those runs are compared with the NCEP/NCAR reanalysis and the US-MEX station precipitation, both of which are available for the period 1948-2004. A compositing technique based on the SST is used that allows us to also compare the results

to the idealized SST runs. Since the leading SST patterns used to force the AGCMs were obtained based on an EOF analysis of *annual* mean SST data (see Schubert et al. 2009), we use the PCs of those same SST patterns to perform a composite analysis of the ensemble mean of the AMIP simulations and the observations. While the Pacific and Atlantic patterns used to force the idealized runs were given a weight of 2 standard deviations, we use here a substantially smaller amplitude (0.5 standard deviations[2]) to do the compositing. This is a compromise between having a sufficient number of cases to provide significant results and keying on the most extreme SST forcing cases that would provide a more consistent comparison with the idealized forcing runs.

Figure 11a shows the composite ensemble mean precipitation and atmospheric circulation anomalies associated with the cold Pacific and warm Atlantic SST patterns. The results are very similar to those based on the idealized runs shown in Fig. 10a though with weaker amplitude. This indicates that any seasonal variations in the SST anomalies associated with the leading SST patterns do not play an important role in the precipitation responses over the U.S.

Figure 11b shows the composite analysis of the observations. In comparing these with the model results (left panels), it is important to remember that the ensemble mean from the model provides a much cleaner estimate of the SST response, whereas the single realization from the observations is subject to considerably more noise from variations that are unrelated to the SST forcing. Nevertheless, the comparison shows a broad consistency between the AMIP ensemble mean and the observations, though there are differences in details. Consistent with the AMIP results, the observed MAM composite

[2] We note that the basic results are not overly sensitive to this choice. For example, values ranging between 0.5 and 1 give fairly similar results.

for the cold Pacific (Fig.11b) shows a wave train emanating from the tropical Pacific onto the North American continent; this includes a weak high over the southern U.S. The observed precipitation anomaly over the U.S. exhibits generally dry conditions over the central and western U.S. as well as over the SE U.S. In JJA, similar to the NSIPP AMIP ensemble mean (Fig.11c), the observed precipitation anomaly (Fig.11d) shows a dry response over the central U.S. and wet responses over regions to the east and southeast. The atmospheric circulation anomaly from the reanalysis is in general consistent with that based on the NSIPP AMIP ensemble mean in that there are a pair of cyclonic circulation anomalies over the tropical Atlantic and a pair of anticyclonic responses over the tropical Pacific, except that the circulation features in the observations are somewhat weaker and are located about 30 to 50 longitudes to the east of those in the NSIPP ensemble mean. The agreement for the warm Atlantic in JAS is rather good. The observations (Fig.11f) show a widespread precipitation deficit over the central and northern U.S. and a precipitation surplus over the eastern and southeastern U.S. Such a precipitation response appears to be associated with the low anomaly centered over the southeastern U.S. Note that the precipitation anomalies in the observations are considerably weaker than those of the NSIPP AMIP ensemble mean (note the use of different color scales). This likely reflects an overall wet bias in the model's precipitation climatology (e.g., Lee et al. 2007). Overall, despite the difference in regional details, the general agreement between the NSIPP ensemble mean and observations suggests that the model produces generally realistic responses to the Pacific and Atlantic SST forcing.

**5. Conclusions**

This study examined the physical mechanisms by which the leading patterns of annual mean SST variability impact U.S. precipitation in the NSIPP-1 AGCM. The focus was on the cold phase of the leading Pacific pattern, and the warm phase of the leading Atlantic pattern, both of which lead to significant drought conditions over the U.S. continent. The precipitation response to the cold Pacific is characterized by deficits over the Great Plains that occur throughout the year but that maximize in summer with a secondary maximum in spring, and weakly pluvial conditions over the SE U.S. during summer. The precipitation response to the warm Atlantic is dominated by persistent deficits over the Great Plains with the maximum deficit occurring in late summer. The warm season precipitation response to the warm Atlantic is overall very similar to the response to the cold Pacific, with however considerably weaker amplitude.

An analysis of the atmospheric moisture budget combined with a stationary wave model diagnosis of the associated atmospheric circulation anomalies was conducted to investigate the mechanisms linking the SST patterns to the anomalies in the U.S. hydroclimate. In particular, the study addressed the reasons for the similarity in the warm season precipitation responses over the Great Plains to the cold Pacific and warm Atlantic, and the causes for the distinct seasonality in the SE U.S. precipitation response to the cold Pacific.

The results show that, for both the cold Pacific and warm Atlantic, the SST-forced precipitation deficits over the Great Plains are associated with substantially reduced atmospheric moisture transport from the Gulf of Mexico to the central U.S., a result of a low-level anomalous cyclonic flow centered over the Gulf of Mexico. The SST forced precipitation deficits over the Great Plains in both cases are greatly amplified by strong

soil moisture feedback in the NSIPP-1 AGCM. It is further shown that the similarity of the responses over the U.S. to the cold Pacific and warm Atlantic is the result of the similarity in the diabatic heating anomalies and low-level anomalous cyclonic flow that develop over the Gulf of Mexico in response to these two spatially distinct SST patterns. In the case of the Atlantic forcing, these heating and circulation responses over the Gulf of Mexico are a direct response to the local prescribed Atlantic SST anomalies, while in the case of the Pacific forcing, these are a secondary response to circulation anomalies forced by the remote diabatic heating anomalies in the tropical Pacific.

The precipitation response to the cold Pacific over the SE U.S. is characterized by substantial seasonal variations with the largest deficit occurring during the spring and weak pluvial conditions occurring during the summer. The summer precipitation increase is the result of the easterly anomaly at the north flank of the already-mentioned anomalous low-level cyclonic flow that develops over the Gulf of Mexico, which in this region acts to increase the moisture transport from the Atlantic to the eastern U.S. In contrast, during spring, the SE U.S. is affected by an upper-tropospheric anomalous high and subsidence that is excited by diabatic heating anomalies in the tropical Pacific. The anomalous high leads to reduced stationary moisture flux convergences. The moderately weakened transient moisture convergences (storm tracks) over the SE U.S. and reduced evaporation play a secondary role. During winter, the precipitation deficit over the SE U.S. is mainly associated with reduced transient moisture flux convergences. The above results help explain the observations that a persistent cold Pacific tends to produce dry conditions during the cold seasons yet wet conditions during summer over the SE U.S.,

leading to the difficulty of sustaining a drought beyond one year there. (Mo and Schemm 2008; Mo et al. 2008).

The above findings are for the most part based on the results of simulations made with the NSIPP-1 AGCM. They are, however, to a large extent similar to those made with other AGCMs participating in the USCLIVAR project, and are generally consistent with the available observations. The models differ most in simulating the *regional details* of the precipitation responses over the U.S. during warm seasons. For example, Fig. 12 shows that, when forced with the warm Atlantic, all five models produce a general precipitation increase and an anomalous low-level cyclonic flow[3] over the NH tropical and subtropical Atlantic in JAS, but they differ in details of the locations and amplitudes. The NSIPP-1 AGCM, the NCAR CCM3 and CAM3.5 have the strongest precipitation increase over the Gulf of Mexico and Caribbean regions, and a secondary precipitation increase over the NH tropical Atlantic, whereas the NCEP GFS has the strongest precipitation response over the NH eastern tropical Pacific and the NH central tropical Atlantic. The GFDL AM2.1 model has the precipitation increases over the Caribbean and the eastern NH tropical Atlantic. Correspondingly, the low-level cyclonic anomalies in the NSIPP AGCM, the NCAR CCM3 and the NCAR CAM3.5 are more localized and well positioned over the Gulf of Mexico, whereas those in the NCEP GFS and the GFDL AM2.1 are centered over the NH tropical Atlantic. This results in different regional atmospheric moisture modulations over the U.S. which, in combination with differences in the land-atmosphere feedback over the U.S. in these models (Koster et al. 2006a), leads to substantially different regional precipitation responses over the U.S.

[3] The geopotential height or streamfunction fields at 850mb are not available from all of the five models. Sea level pressure is used instead to illustrate the low-level atmospheric circulation responses.

This study highlights the potential importance of the Gulf of Mexico and more generally the Intra-America Seas in shaping the precipitation responses to both Pacific and Atlantic SST anomalies. The study also highlights the need to substantially improve the current generation of models in representing the warm season responses of tropical convection and atmospheric circulations, as well as in representing the strength of the land-atmosphere feedbacks.

**Acknowledgements**

This study is supported by the NOAA Climate Prediction Program for the Americas (CPPA) and the NASA Modeling, Analysis, and Prediction (MAP) program. The authors would like to thank NASA's Global Modeling and Assimilation Office (GMAO) for making the NSIPP1 runs available, the Lamont-Doherty Earth Observatory of Columbia University for making their CCM3 runs available, NOAA's Climate Prediction Center (CPC)/Climate Test Bed (CTB) for making the GFS runs available, NOAA's Geophysical Fluid Dynamics Laboratory (GFDL) for making the AM2.1 runs available, the National Center for Atmospheric Research (NCAR) for making the CAM3.5 runs available, and the Center for Ocean Land Atmosphere (COLA) and the University of Miami's Rosenstiel School of Marine and Atmospheric Science for making the CCSM3.0 coupled model runs available.

**References**

Bacmeister J., P. J. Pegion, S. D. Schubert, and M. J. Suarez, 2000: An atlas of seasonal means simulated by the NSIPP 1 atmospheric GCM. *Vol.* 17. NASA Tech. Memo. 104606, Goddard Space Flight Center, Greenbelt, MD, 194 pp.

Barlow, M., S. Nigam, and E.H. Berbery, 2001: ENSO, Pacific Decadal Variability, and U.S. summertime precipitation, drought, and streamflow. *J. Climate*, **14**, 2105-2128.

Campana, K. and P. Caplan, Editors, 2005: Technical Procedure Bulletin for T382 Global Forecast System (http://www.emc.ncep.noaa.gov/gc_wmb/Documentation/TPBoct05/T382.TPB.FINAL.htm).

Delworth and co-authors, 2006: GFDL's CM2 global coupled climate models - Part 1: Formulation and simulation characteristics. *J. Climate*, **19**, 643-674.

Enfield, D., Mestas-Nuñez, A.M., and Trimble, P.J., 2001, The Atlantic multidecadal oscillation and its relation to rainfall and river flows in the continental U.S. *Geophys. Res. Lett.*, **28**, 2077-2080.

Held, I. M., M. Ting, and H. Wang, 2002: Northern winter stationary waves: theory and modeling. *J. Climate*, **15**, 2125-2144.

Higgins R. W., A. Leetmaa, Y. Xue, and A. Barnston, 2000: Dominant factors influencing the seasonal predictability of U.S. precipitation and surface air temperature. *J. Climate*, **13**, 3994–4017.

Hoerling M. P., and A. Kumar, 2003: The perfect ocean for drought. *Science*, **299**, 691–694.

Kalnay E. and co-authors, 1996: The NCEP/NCAR 40-year reanalysis project. *Bull. Amer. Meteor. Soc.*, **77**, 437-470.

Kiehl, J.T., J.J. Hack, G. Bonan, B.A. Boville, D. Williamson and P. Rasch, 1998: The National Center for Atmospheric Research Community Climate Model: CCM3. *J. Climate*, **11**, 1131-1149.

Koster, R. D., M. J. Suarez, and M. Heiser, 2000: Variance and predictability of precipitation at seasonal-to-interannual timescales. *J. Hydrometeor*, **1**, 26-46.

Koster, R. D., M. J. Suarez, R. W. Higgins, and H. M. van den Dool, 2003: Observational evidence that soil moisture variations affect precipitation. *Geophys. Res. Lett*., **30**, 1241, doi:10.1029/2002GL016571.

Koster, R. D., and M. J. Suarez, 2004: Suggestions in the observational record of land-atmosphere feedback operating at seasonal time scales. *J. Hydrometeor.*, **5**, 567-572.

Koster, R.D. and Coauthors, 2006a: GLACE: The Global Land–Atmosphere Coupling Experiment. Part I: Overview. *J. Hydrometeor.*, **7**, 590–610.

Koster, R. D., M. J. Suarez, and S. D. Schubert, 2006b: Distinct hydrological signatures in observed historical temperature fields. *J. Hydrometeor.*, **7**, 1061-1074.

Lau N.-C., A. Leetmaa, M.J. Nath, and H-L. Wang, 2005: Influences of ENSO-induced Indo-Western Pacific SST anomalies on extratropical atmospheric variability during the Boreal summer. *J. Climate,* **18**, 2922-2942.

Lee, M.-I., S. D. Schubert, M. J. Suarez, T. Bell, K.-M. Kim, 2007: The Diurnal Cycle of Precipitation in the NASA/NSIPP Atmospheric General Circulation Model, *J. Geophys. Res*., 112, D16111, doi:10.1029/2006JD008346.

McCabe, G.J., Palecki, M.A., and Betancourt, J.L, 2004: Pacific and Atlantic Ocean influences on multidecadal drought frequency in the United States. *Proc. Nat. Acad. Sci.*, **101**, 4136-4141.

Mo, K. C., and J. E. Schemm, 2008: Relationships between ENSO and drought over the southeastern United States, *Geophys. Res. Lett.*, **35**, L15701, doi:10.1029/2008GL034656.

Mo, K. C., J. E. Schemm, and S.-H. Yoo, 2008: Influence of ENSO and the Atlantic multi-decadal oscillation on drought over the United States. *J. Climate*, in press.

Namias J., 1983: Some Causes of United States Drought. *J. Appl. Meteor.*, **22**, 30–39.

Nigam, S., and A. Ruiz-Barradas, 2006: Seasonal hydroclimate variability over North America in Global and Regional Reanalyses and AMIP Simulations: Varied representation. *J. Climate*, **19**, 815-837.

Oleson, K. W. and Coauthors, 2008: Improvements to the Community Land Model and their impact on the hydrological cycle. *J. Geophys. Res.*, **113**, G01021, doi:10.1029/2007JG000563.

Pegion, P., S. Schubert, and M. J. Suarez, 2000: An assessment of the predictability of northern winter seasonal means with the NSIPP1 AGCM. *NASA Tech. Memo-2000-104606*, Vol. 18, 100pp.

Rayner, N. A., D. E. Parker, E. B. Horton, C. K. Folland, L. V. Alexander, D. P. Rowell, E. C. Kent, and A. Kaplan, 2003: Global analyses of sea surface temperature, sea ice, and night marine air temperature since the late nineteenth century. *J. Geophys. Res.*, **99**, 20323-20344.

Roads J., M. Kanamitsu, and R. Stewart, 2002: CSE water and energy budgets in the NCEP–DOE Reanalysis II. *J. Hydrometeor*, **3**, 227–248

Ropelewski C. F., and M. S. Halpert, 1986: North American precipitation and temperature patterns associated with the El Niño–Southern Oscillation (ENSO). *Mon. Wea. Rev.*, **114**, 2352–2362.

Seager, R., Y. Kushnir, C. Herweijer, N. Naik and J. Velez (Nakamura), 2005: Modeling of tropical forcing of persistent droughts and pluvials over western North America: 1856-2000. *J. Climate*, **18**, 4065-4088.

Seager, R., N. Graham, C. Herweijer, A. L. Gordon, Y. Kushnir and E. Cook, 2007: Blueprints for Medieval hydroclimate. *Quaternary Science Reviews*, **26**(19-21): doi:10.1016/j.quascirev.2007.04.020, 2322-2336.

Schubert S. D., M. J. Suarez, P. J. Pegion, M. A. Kistler, and A. Kumer, 2002: Predictability of zonal means during boreal summer. *J. Climate*, **15**, 420–434.

Schubert S. D., M. J. Suarez, P. J. Pegion, R. D. Koster, and J. T. Bacmeister, 2004a: Causes of long-term drought in the U.S. Great Plains. *J. Climate*, **17**, 485–503.

Schubert S. D., M. J. Suarez, P. J. Pegion, R. D. Koster, and J. T. Bacmeister, 2004b: On the cause of the 1930s dust bowl. *Science*, **303**, 1855–1859.

Schubert S., and Coauthors, 2009: A USCLIVAR Project to Assess and Compare the Responses of Global Climate Models to Drought-Related SST Forcing Patterns: Overview and Results. *J. Climate,* in press.

Stockli, R. and Coauthors, 2008: Use of FLUXNET in the Community Land Model development, *J. Geophys. Res.*, **113**, G01025, doi:10.1029/2007JG000562.

Sutton, R. T.; Hodson, L. R., 2005: Atlantic forcing of North American and European summer climate. *Science,* **309**: 115–118.

Ting, M. and H. Wang, 1997: Summertime U.S. precipitation variability and its relation to Pacific Sea Surface Temperature. *J. Climate*, **10**,1853-1873.

Ting, M. and L. Yu, 1998: Steady response to tropical heating in wavy linear and nonlinear baroclinic models. *J. Atmos. Sci.,* **55**, 3565–3582.

Ting, M. F., H. L. Wang and L. H. Yu, 2001: Nonlinear stationary wave maintenance and seasonal cycle in the GFDL R30 GCM. *J. Atmos. Sci*., **58**, 2331-2354.

Wang, H., S. Schubert, M. Suarez, J. Chen, M. Hoerling, A. Kumar and P. Pegion, 2009: Attribution of Seasonality and Regionality of Climate Trends over the United States during 1950-2000. *J. Climate*, **22**, 2571–2590,.

Zhang, Y., J.M. Wallace, D.S. Battisti, 1997: ENSO-like interdecadal variability: 1900-93. *J. Climate*, **10**, 1004-1020.

**Figure Captions**

Figure 1. Seasonal mean precipitation responses (mm/day) to the (a) warm Pacific, (b) cold Pacific, (c) warm Atlantic, (d) cold Atlantic and (e) warm Trend SST patterns, for December-February (DJF), March-May (MAM), June-August (JJA) and September-November (SON) in the idealized experiments performed using the NASA NSIPP-1 AGCM. The precipitation responses are obtained by averaging the differences between the anomaly runs and the control run over the last 80 years (50 years for the warm Trend). Regions with responses that are significant at the 5% level based on a *t* test are indicated using contours.

Figure 2. Seasonality of precipitation responses (mm/day) averaged over (a) the U.S. Great Plains (255°E-265°E, 30°N-50°N) and (b) the southeast (SE) U.S. (267°E-290°E, 24°N-36°N) for the warm Pacific, cold Pacific, warm Atlantic, cold Atlantic, and warm Trend SST patterns in the idealized experiments performed using the NASA NSIPP-1 AGCM. The lines for SST patterns that induce general drought (pluvial) conditions are marked with closed (open) circles. Three-month running mean values are shown.

Figure 3. Seasonality of precipitation response (black line with open circle), evaporation response (blue line with closed square), changes in vertically integrated transient moisture flux convergences ( $qconv'_{tran}$ ) (green line with closed circle), changes in vertically integrated stationary moisture flux convergences ( $qconv'_{stat}$ ) (red line with open square) and those due to changes in atmospheric circulation ( $qconv'_{statV}$ ) (dashed magenta line with multiplication sign) and changes in atmospheric moisture ( $qconv'_{statQ}$ ) (dashed dark yellow line with open circle), in response to the cold Pacific

SST pattern over (a) the SE U.S., (b) the Great Plains, and those in response to the warm Atlantic pattern over (c) the Great Plains. Three-month running mean values are shown. Units: mm/day.

Figure 4. Atmospheric moisture budget analysis for MAM response to cold Pacific pattern in (a) the standard idealized run, and (b) the auxiliary run that has the soil moisture feedback turned off, performed using the NSIPP-1 AGCM. The responses of precipitation with vertical velocity (ω) in pressure coordinates at 300mb (contour), evaporation, vertically integrated transient moisture flux convergences ( $qconv'_{tran}$ ), vertically integrated stationary moisture flux convergences due to changes in atmospheric moisture ( $qconv'_{statQ}$ ), and those due to the changes in atmospheric circulation ( $qconv'_{statV}$ ) superimposed with the corresponding vertically integrated stationary moisture fluxes, are shown. Note that the ω anomaly in MAM reaches its maximum at about 300mb over the Great Plains. Units: mm/day.

Figure 5. The MAM eddy streamfunction ( $m^2 s^{-1}$ ) at $\sigma$ =0.257 in (a) the AGCM response to the cold Pacific SST pattern, and the stationary wave model responses to (b) the sum of diabatic heating anomalies and anomalies in transient flux convergences, (c) the diabatic heating anomalies only, (d) the transient flux convergence anomalies only, (e) the MAM mean diabatic heating anomalies imposed on DJF mean 3-D background state, (f) the DJF mean diabatic heating anomalies imposed on MAM mean 3-D background state. The vertically integrated diabatic heating anomalies (K/day) are shaded in all panels except (d). Contour interval of streamfunction is $1\times10^6 m^2 s^{-1}$ (negative values are dashed and the zero line is the first solid contour).

Figure 6. Atmospheric moisture budget analysis for JJA response to cold Pacific pattern in (a) the standard idealized run, and (b) the auxiliary run that has the soil moisture feedback disabled, performed using the NSIPP-1 AGCM. The responses of precipitation, evaporation, vertically integrated transient moisture flux convergences ($qconv'_{tran}$), vertically integrated stationary moisture flux convergences due to changes in atmospheric moisture ($qconv'_{statQ}$), and those due to the changes in atmospheric circulation ($qconv'_{statV}$) superimposed with the corresponding vertically integrated stationary moisture fluxes, are shown. Units: mm/day.

Figure 7. The JJA eddy streamfunction ($m^2 s^{-1}$) at $\sigma$=0.866 in (a) the AGCM response to the cold Pacific SST pattern, and the stationary wave model response to (b) the sum of diabatic heating anomalies and anomalies in transient flux convergences, (c) the diabatic heating anomalies only, and regional diabatic heating anomalies over (d) the Gulf of Mexico and U.S., (e) the Pacific, and (f) the Gulf of Mexico. The corresponding vertically integrated diabatic heating anomalies (K/day) are shaded. Contour interval of streamfunction is $0.5\times10^6 m^2 s^{-1}$ (negative values are dashed and the zero line is the first solid contour).

Figure 8. Same as Fig.6 but for the July-September (JAS) responses to warm Atlantic.

Figure 9. The JAS eddy streamfunction ($m^2 s^{-1}$) at $\sigma$=0.866 in (a) the AGCM response to the warm Atlantic SST pattern, and the stationary wave model response to (b) the sum of diabatic heating anomalies and anomalies in transient flux convergences, (c) the diabatic heating anomalies, and (d) the diabatic heating anomalies over the Gulf of Mexico, U.S. and the NH tropical Atlantic. The corresponding vertically integrated

diabatic heating anomalies (K/day) are shaded. Contour interval of streamfunction is $0.5\times10^6 m^2 s^{-1}$ (negative values are dashed and the zero line is the first solid contour).

Figure 10. Left panels show the results based on the NSIPP-1 AGCM: (a) MAM mean responses of precipitation (mm/day) and eddy streamfunction ($m^2 s^{-1}$) at $\sigma$=0.257 to the cold Pacific SST pattern, (b) JJA mean responses of precipitation and eddy streamfunction at $\sigma$=0.866 to the cold Pacific SST pattern, (c) JAS mean responses of precipitation and eddy streamfunction at $\sigma$=0.866 to the warm Atlantic SST pattern. The right panels are the same as the left panels but for the four-model ensemble mean responses of the idealized runs by the NCEP GFS, the NCAR CCM3, the NCAR CAM3.5 and the GFDL AM2.1. Contour intervals of streamfunction are $1\times10^6 m^2 s^{-1}$ in (a)-(b) and $0.5\times10^6 m^2 s^{-1}$ in (c)-(f) (negative values are dashed and the zero line is the first solid contour).

Figure 11. The MAM mean precipitation (mm/day) and eddy streamfunction ($m^2 s^{-1}$) anomalies at $\sigma$=0.257 associated with the cold Pacific SST pattern in (a) the NSIPP-1 AMIP ensemble mean simulation, and (b) the observations; the precipitation and eddy streamfunction anomalies at $\sigma$=0.866 associated with the (c) cold Pacific in JJA and (e) warm Atlantic in JAS in the NSIPP-1 AMIP ensemble mean simulation, and associated with the (d) cold Pacific in JJA and (f) warm Atlantic in JAS in the observations. The threshold of 0.5 standard deviation of the PCs of leading SST patterns is used. Note the use of different color scales for the precipitation in the NSIPP AMIP ensemble mean and the observations. Contour intervals of streamfunction are $0.4\times10^6 m^2 s^{-1}$ in (a)-(b) and $0.2\times10^6 m^2 s^{-1}$ in (c)-(f) (negative values are dashed and the zero line is the first solid contour).

Figure 12. The JAS mean precipitation (mm/day) (shaded) and sea level pressure (millibar) (contour) responses to the warm Atlantic SST pattern in the idealized runs with the five AGCMs. Contour interval of the sea level pressure is 0.3millibar (negative values are dashed and the zero line is the first solid contour).

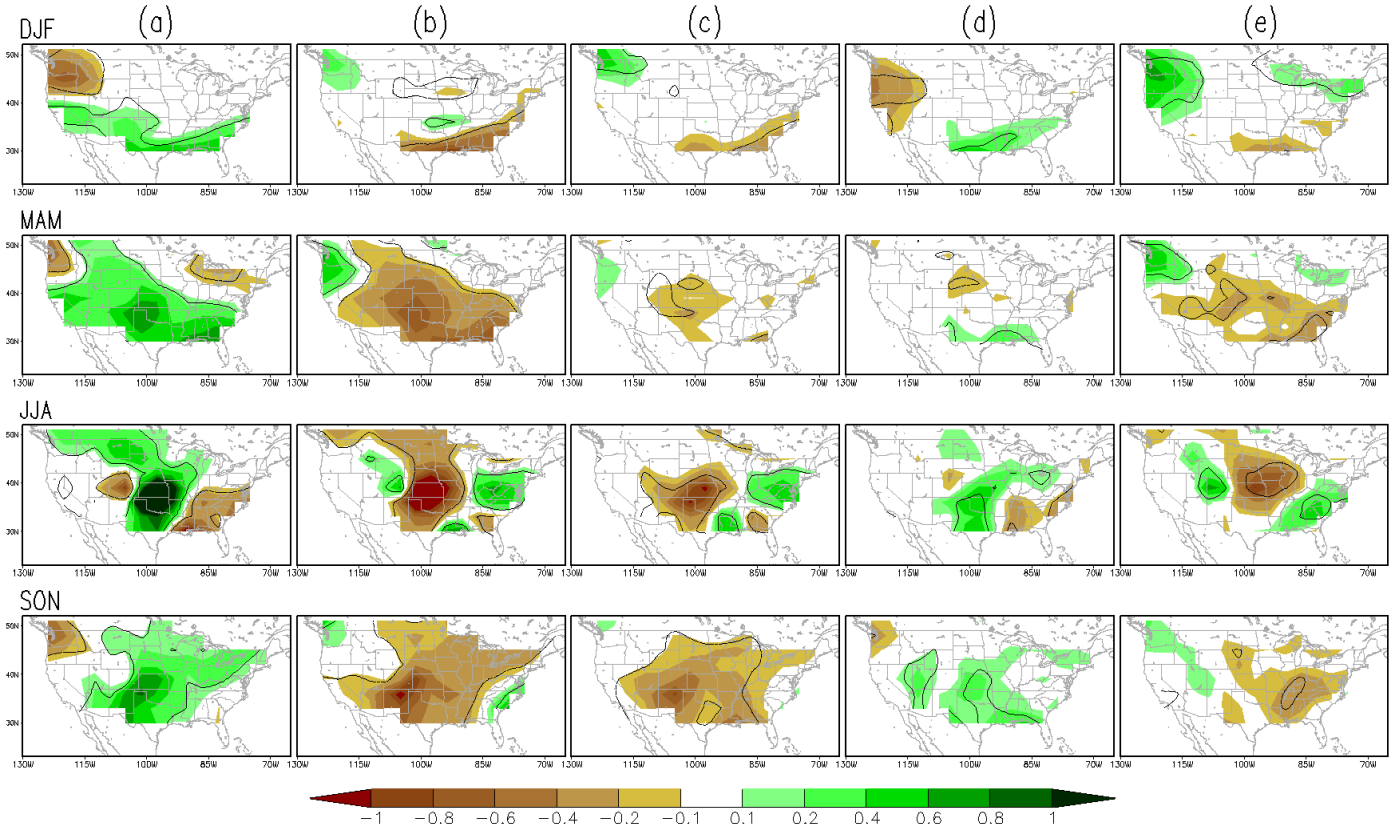


Figure 1. Seasonal mean precipitation responses (mm/day) to the (a) warm Pacific, (b) cold Pacific, (c) warm Atlantic, (d) cold Atlantic and (e) warm Trend SST patterns, for December-February (DJF), March-May (MAM), June-August (JJA) and September-November (SON) in the idealized experiments performed using the NASA NSIPP-1 AGCM. The precipitation responses are obtained by averaging the differences between the anomaly runs and the control run over the last 80 years (50 years for the warm Trend). Regions with responses that are significant at the 5% level based on a *t* test are indicated using contours.

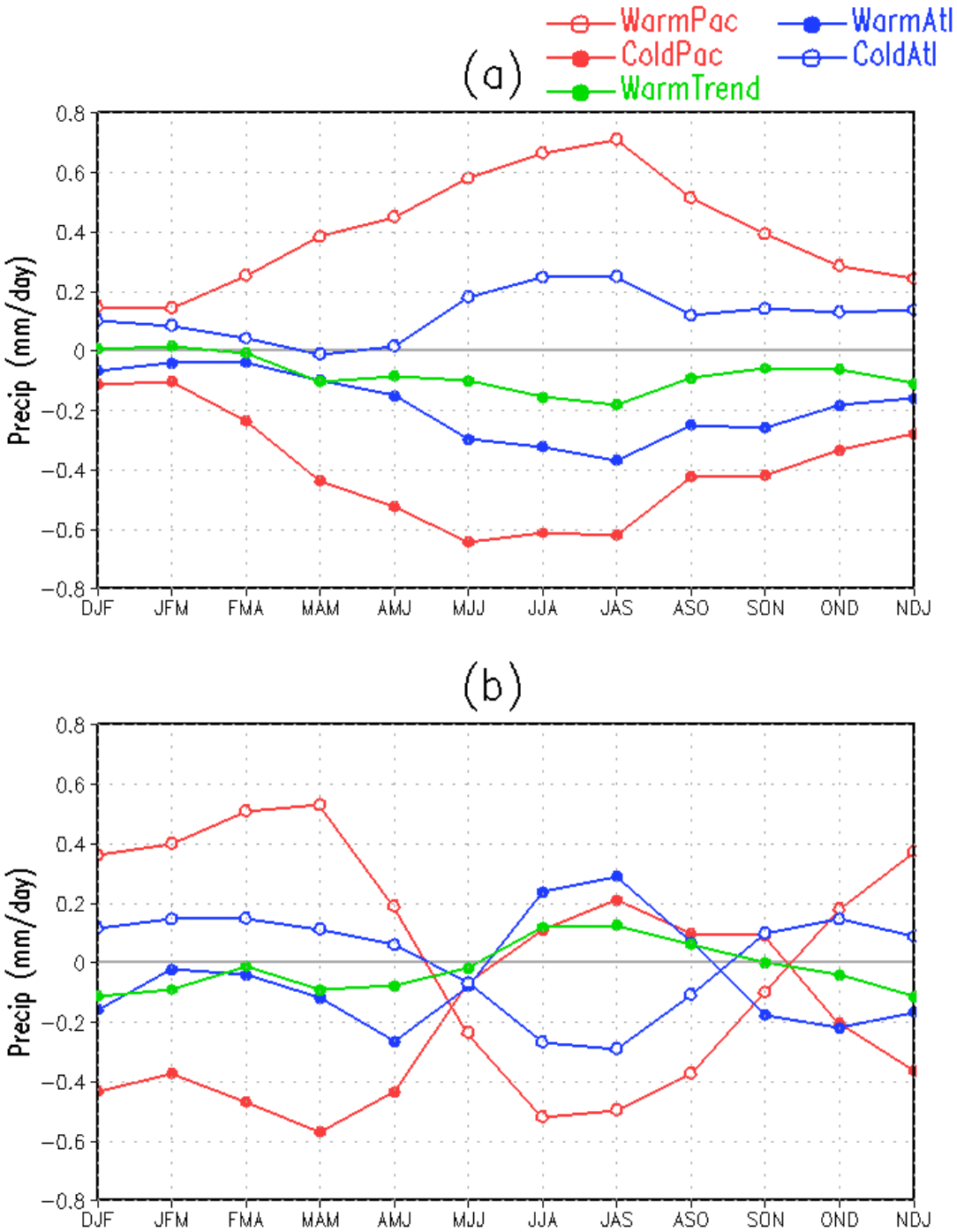


Figure 2. Seasonality of precipitation responses (mm/day) averaged over (a) the U.S. Great Plains (255°E-265°E, 30°N-50°N) and (b) the southeast (SE) U.S. (267°E-290°E, 24°N-36°N) for the warm Pacific, cold Pacific, warm Atlantic, cold Atlantic, and warm Trend SST patterns in the idealized experiments performed using the NASA NSIPP-1 AGCM. The lines for SST patterns that induce general drought (pluvial) conditions are marked with closed (open) circles. Three-month running mean values are shown.

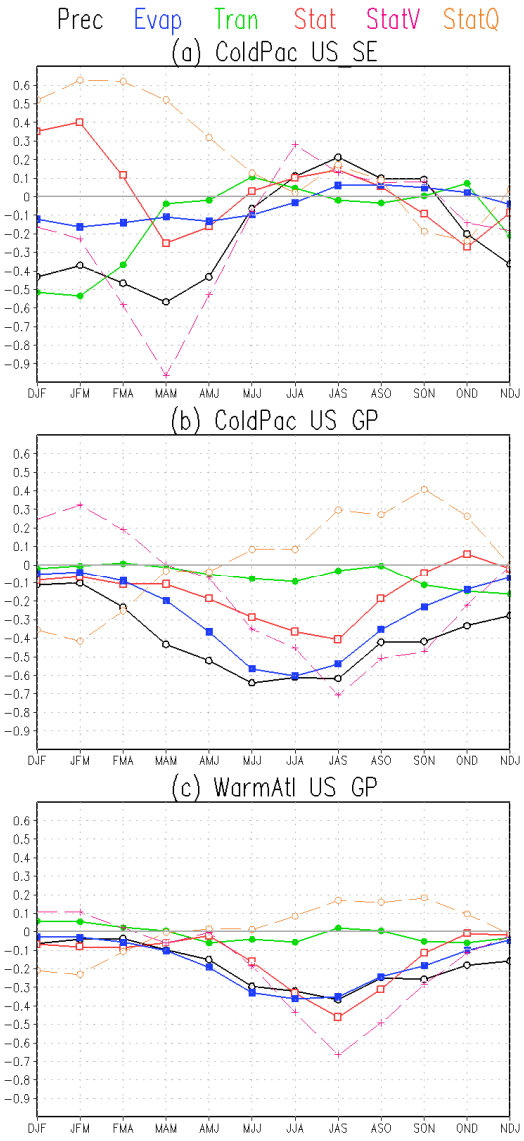


Figure 3. Seasonality of precipitation response (black line with open circle), evaporation response (blue line with closed square), changes in vertically integrated transient moisture flux convergences ( $qconv'_{tran}$ ) (green line with closed circle), changes in vertically integrated stationary moisture flux convergences ( $qconv'_{stat}$ ) (red line with open square) and those due to changes in atmospheric circulation ( $qconv'_{statV}$ ) (dashed magenta line with multiplication sign) and changes in atmospheric moisture ( $qconv'_{statQ}$ ) (dashed dark yellow line with open circle), in response to the cold Pacific SST pattern over (a) the SE U.S., (b) the Great Plains, and those in response to the warm Atlantic pattern over (c) the Great Plains. Three-month running mean values are shown. Units: mm/day.

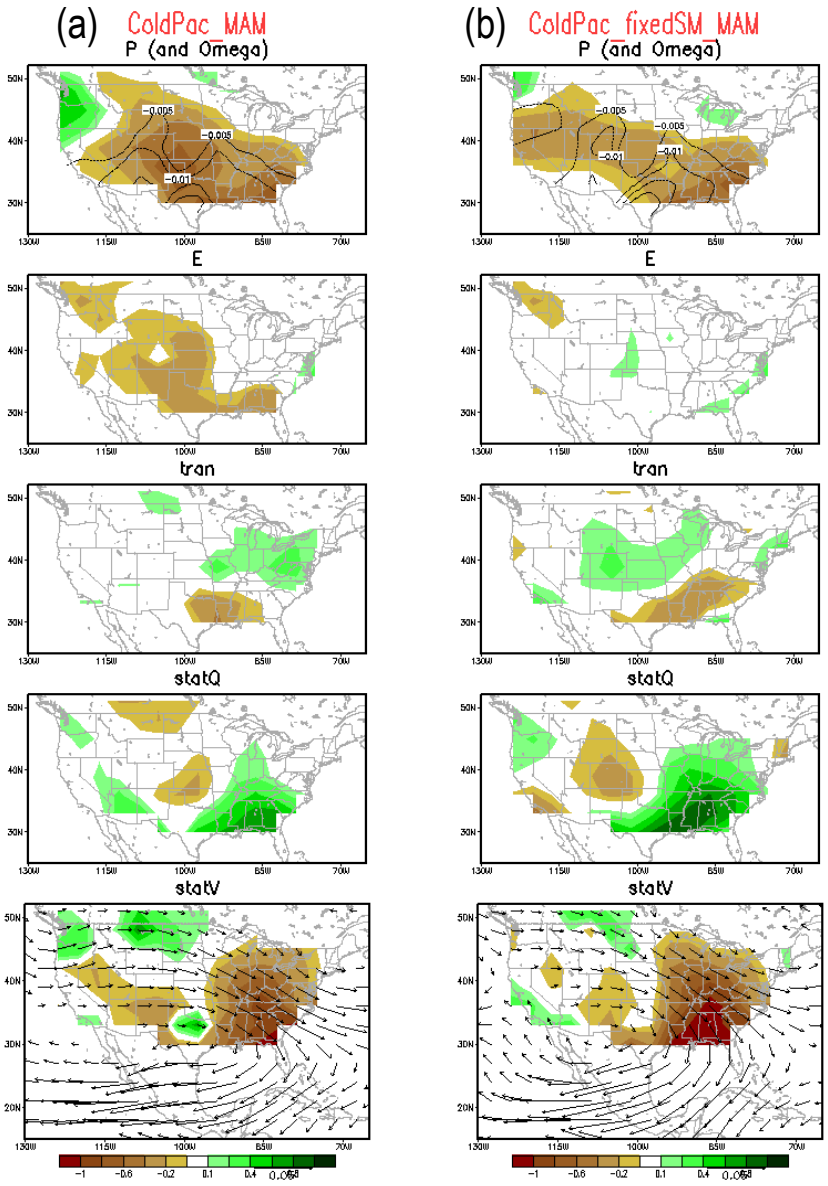


Figure 4. Atmospheric moisture budget analysis for MAM response to cold Pacific pattern in (a) the standard idealized run, and (b) the auxiliary run that has the soil moisture feedback turned off, performed using the NSIPP-1 AGCM. The responses of precipitation with vertical velocity (ω) in pressure coordinates at 300mb (contour), evaporation, vertically integrated transient moisture flux convergences ( $qconv'_{tran}$ ), vertically integrated stationary moisture flux convergences due to changes in atmospheric moisture ( $qconv'_{statQ}$ ), and those due to the changes in atmospheric circulation ( $qconv'_{statV}$ ) superimposed with the corresponding vertically integrated stationary moisture fluxes, are shown. Note that the ω anomaly in MAM reaches its maximum at about 300mb over the Great Plains. Units: mm/day.

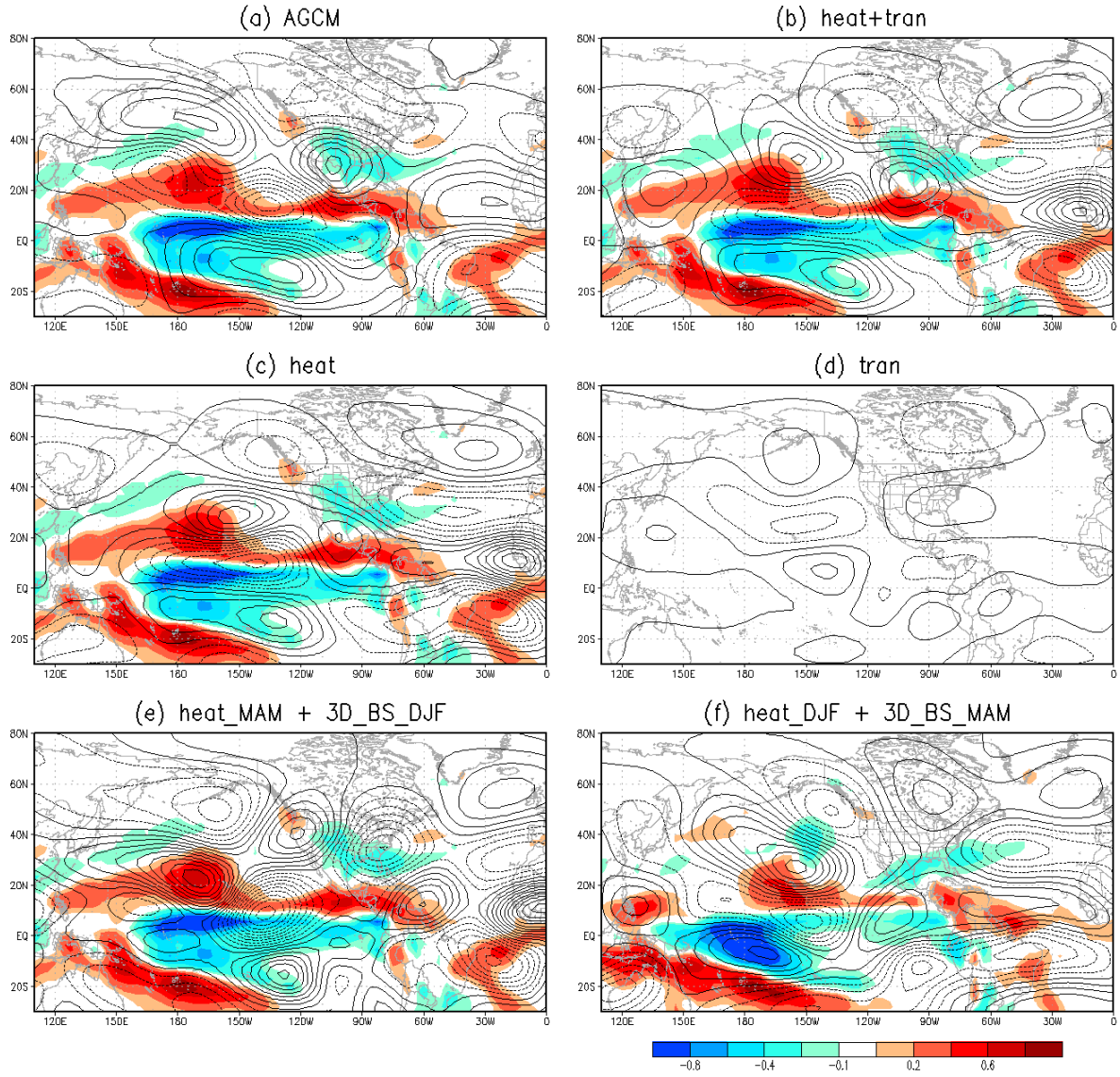


Figure 5. The MAM eddy streamfunction ( $m^2 s^{-1}$ ) at $\sigma$ =0.257 in (a) the AGCM response to the cold Pacific SST pattern, and the stationary wave model responses to (b) the sum of diabatic heating anomalies and anomalies in transient flux convergences, (c) the diabatic heating anomalies only, (d) the transient flux convergence anomalies only, (e) the MAM mean diabatic heating anomalies imposed on DJF mean 3-D background state, (f) the DJF mean diabatic heating anomalies imposed on MAM mean 3-D background state. The vertically integrated diabatic heating anomalies (K/day) are shaded in all panels except (d). Contour interval of streamfunction is $1\times10^6 m^2 s^{-1}$ (negative values are dashed and the zero line is the first solid contour).

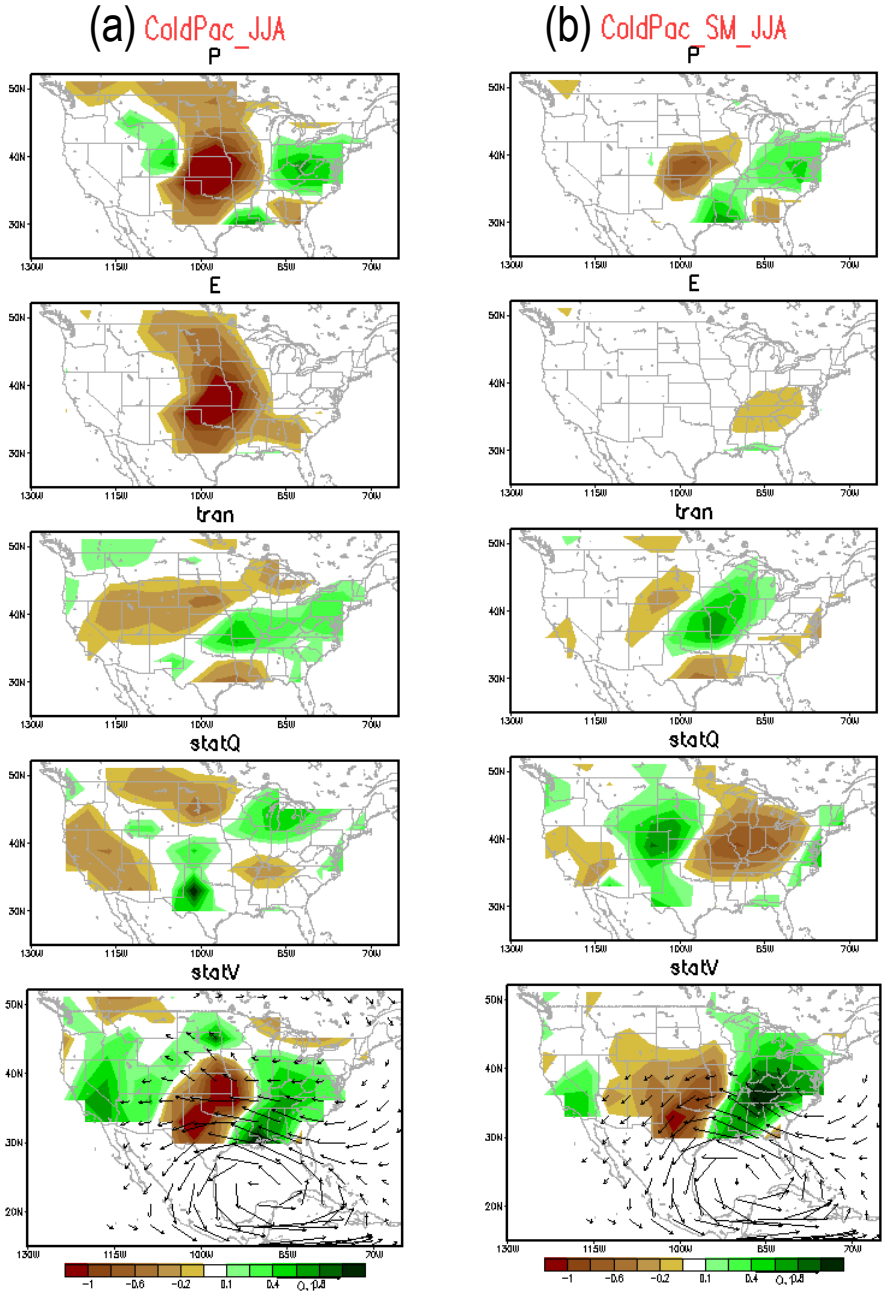


Figure 6. Atmospheric moisture budget analysis for JJA response to cold Pacific pattern in (a) the standard idealized run, and (b) the auxiliary run that has the soil moisture feedback disabled, performed using the NSIPP-1 AGCM. The responses of precipitation, evaporation, vertically integrated transient moisture flux convergences ( $qconv'_{tran}$ ), vertically integrated stationary moisture flux convergences due to changes in atmospheric moisture ( $qconv'_{statQ}$ ), and those due to the changes in atmospheric circulation ( $qconv'_{statV}$ ) superimposed with the corresponding vertically integrated stationary moisture fluxes, are shown. Units: mm/day.

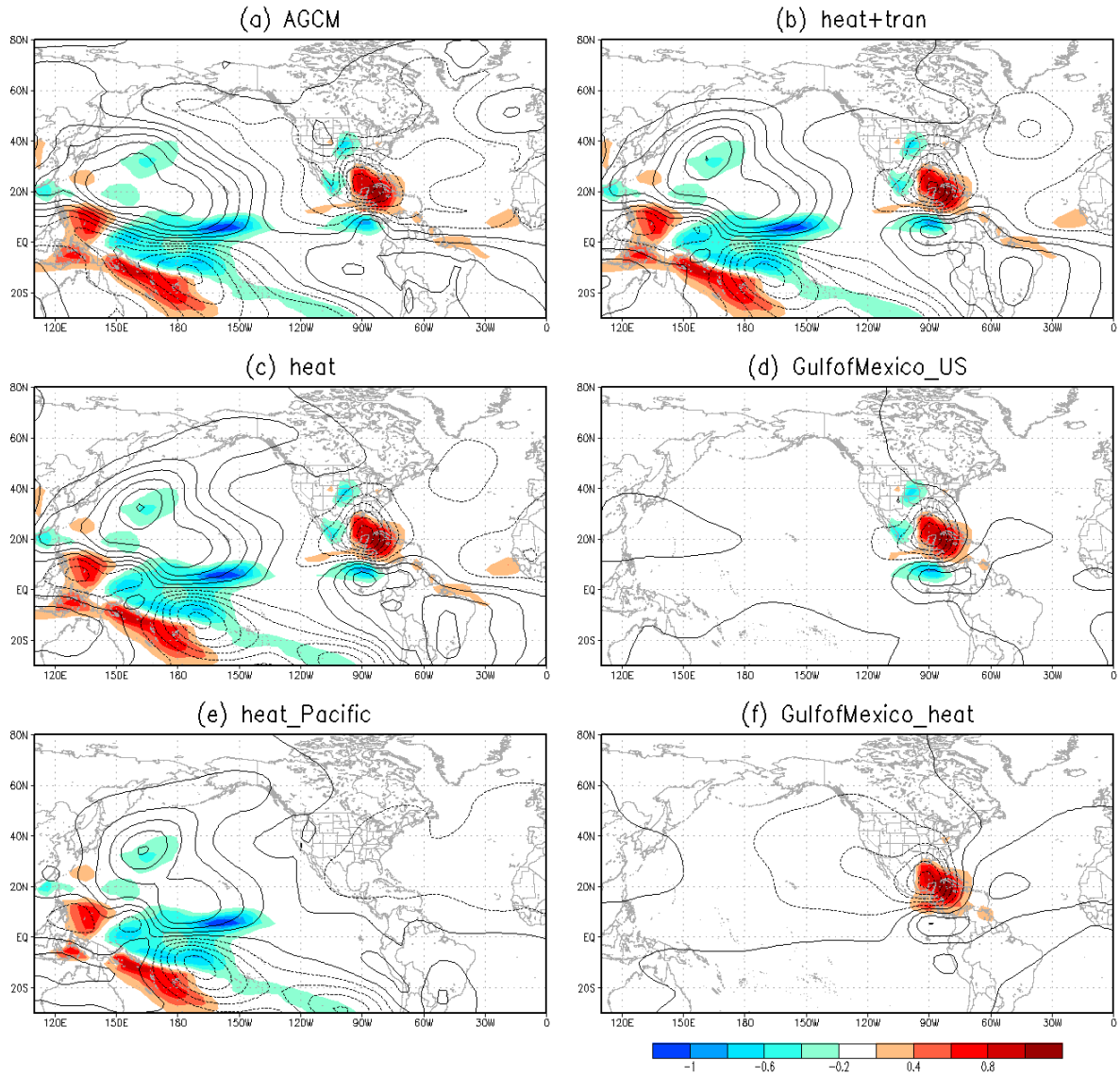


Figure 7. The JJA eddy streamfunction ( $m^2 s^{-1}$ ) at $\sigma$ =0.866 in (a) the AGCM response to the cold Pacific SST pattern, and the stationary wave model response to (b) the sum of diabatic heating anomalies and anomalies in transient flux convergences, (c) the diabatic heating anomalies only, and regional diabatic heating anomalies over (d) the Gulf of Mexico and U.S., (e) the Pacific, and (f) the Gulf of Mexico. The corresponding vertically integrated diabatic heating anomalies (K/day) are shaded. Contour interval of streamfunction is $0.5\times10^6 m^2 s^{-1}$ (negative values are dashed and the zero line is the first solid contour).

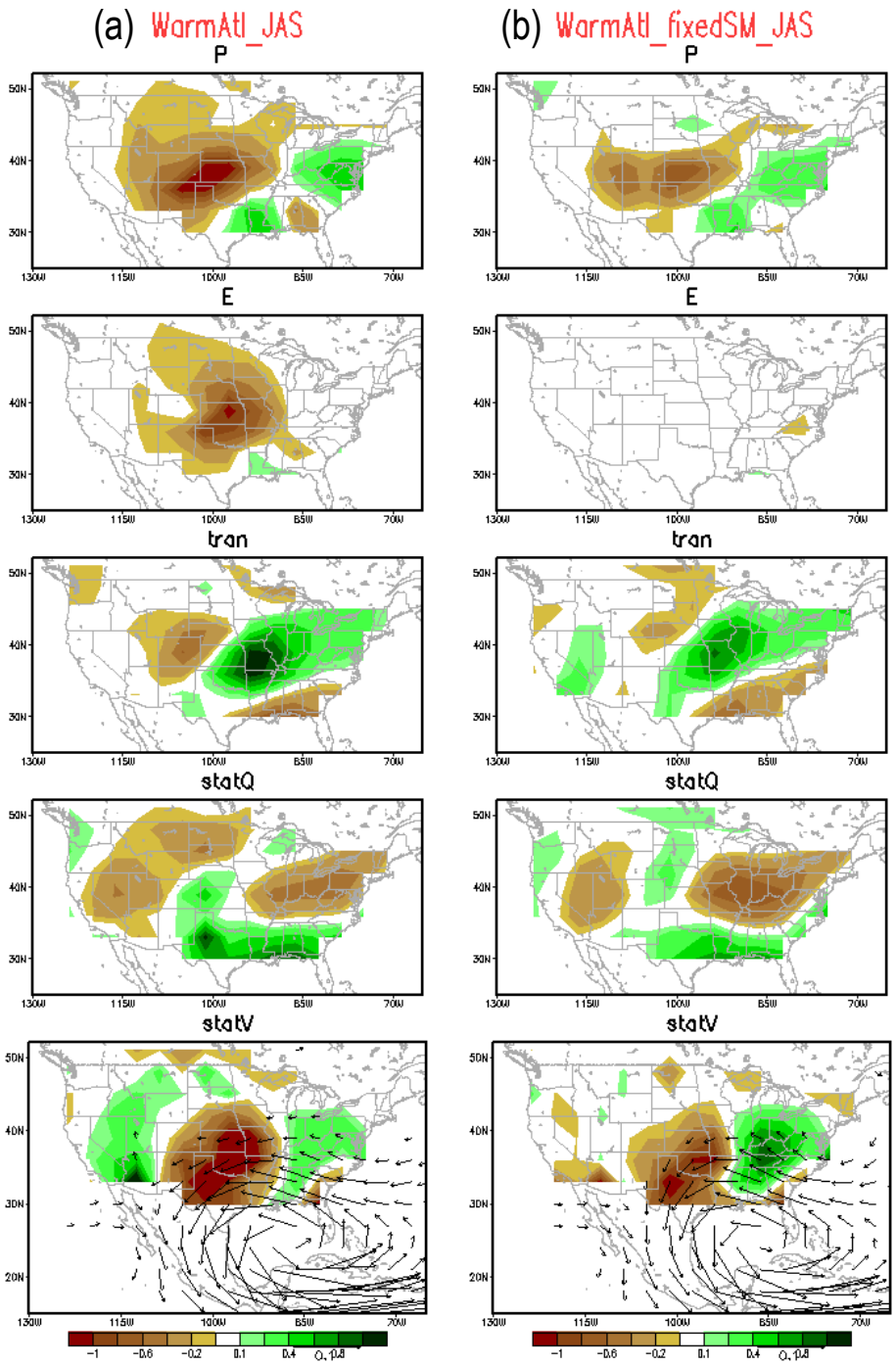


Figure 8. Same as Fig.6 but for the July-September (JAS) responses to warm Atlantic.

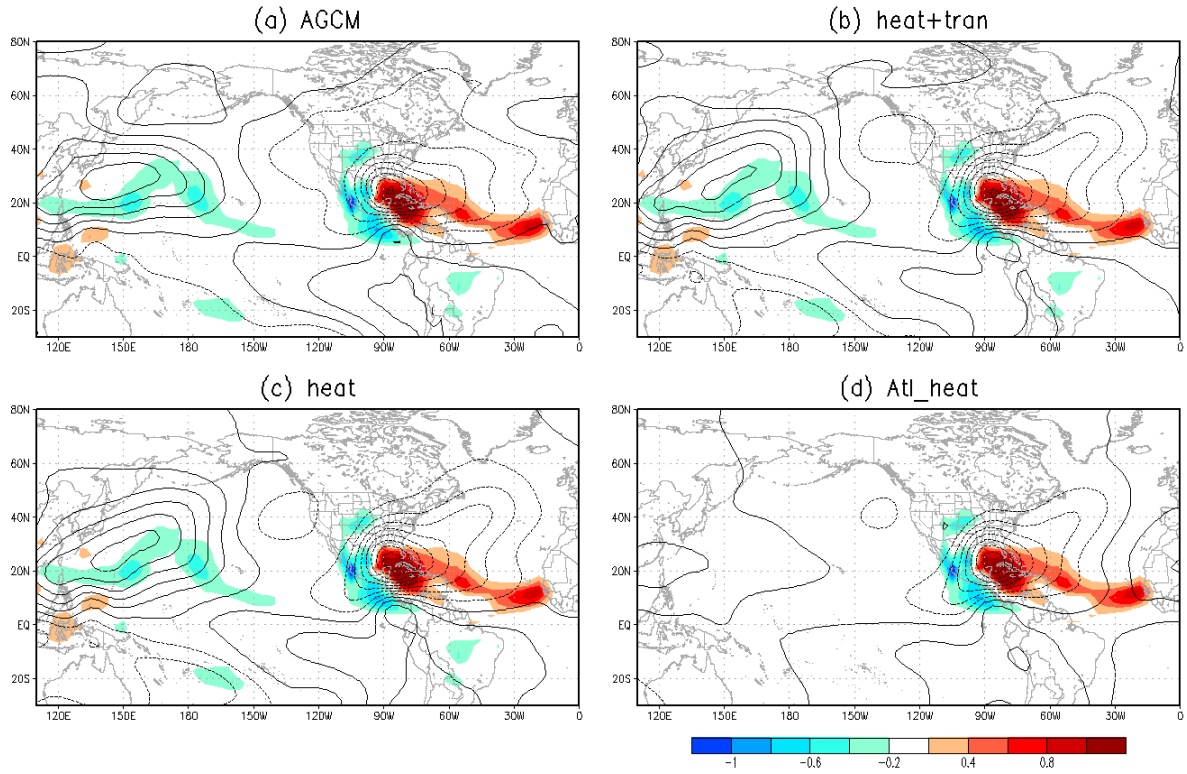


Figure 9. The JAS eddy streamfunction ( $m^2 s^{-1}$ ) at $\sigma$ =0.866 in (a) the AGCM response to the warm Atlantic SST pattern, and the stationary wave model response to (b) the sum of diabatic heating anomalies and anomalies in transient flux convergences, (c) the diabatic heating anomalies, and (d) the diabatic heating anomalies over the Gulf of Mexico, U.S. and the NH tropical Atlantic. The corresponding vertically integrated diabatic heating anomalies (K/day) are shaded. Contour interval of streamfunction is $0.5\times10^6 m^2 s^{-1}$ (negative values are dashed and the zero line is the first solid contour).

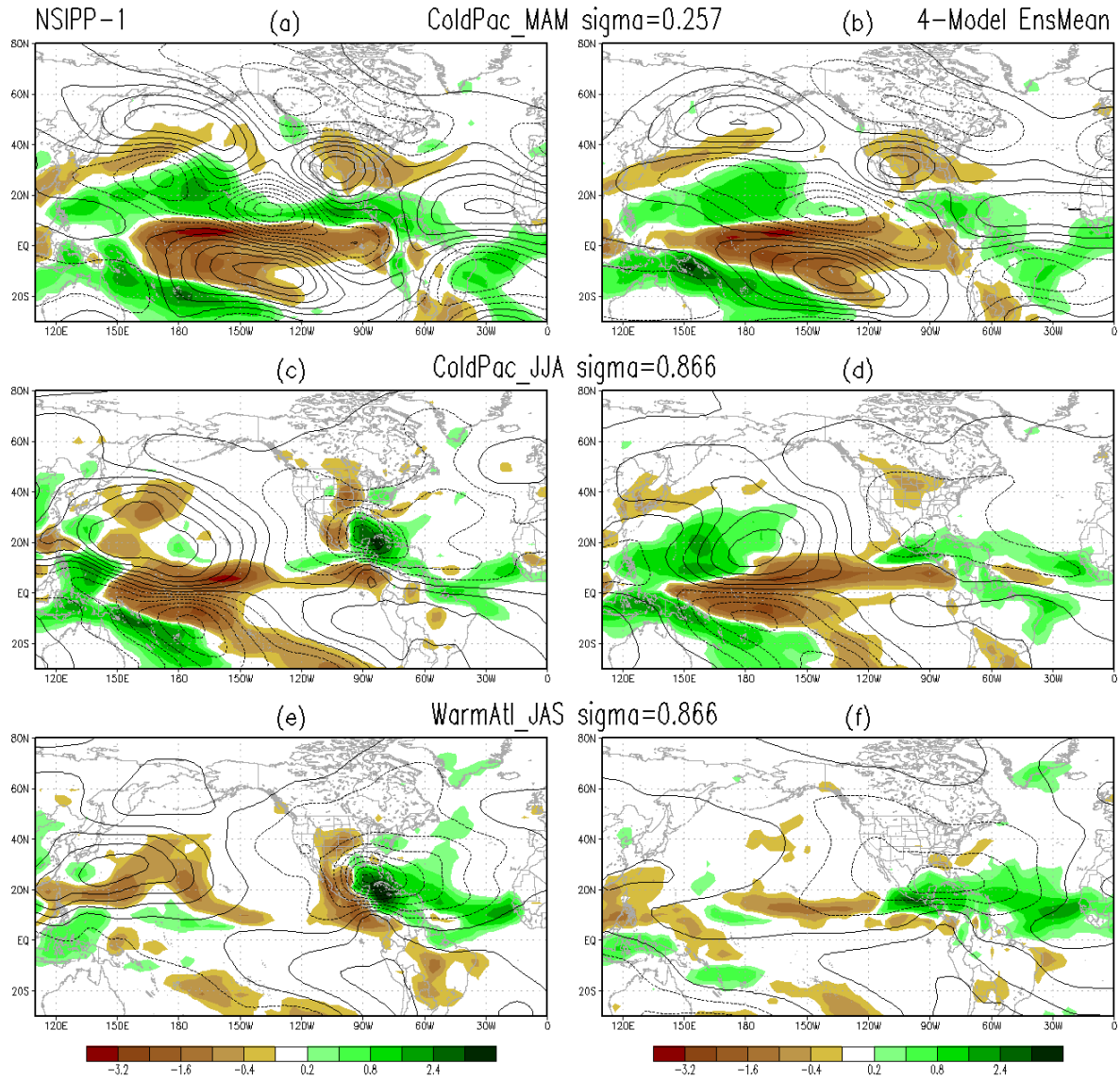


Figure 10. Left panels show the results based on the NSIPP-1 AGCM: (a) MAM mean responses of precipitation (mm/day) and eddy streamfunction ($m^2 s^{-1}$) at $\sigma$=0.257 to the cold Pacific SST pattern, (b) JJA mean responses of precipitation and eddy streamfunction at $\sigma$=0.866 to the cold Pacific SST pattern, (c) JAS mean responses of precipitation and eddy streamfunction at $\sigma$=0.866 to the warm Atlantic SST pattern. The right panels are the same as the left panels but for the four-model ensemble mean responses of the idealized runs by the NCEP GFS, the NCAR CCM3, the NCAR CAM3.5 and the GFDL AM2.1. Contour intervals of streamfunction are $1\times10^6 m^2 s^{-1}$ in (a)-(b) and $0.5\times10^6 m^2 s^{-1}$ in (c)-(f) (negative values are dashed and the zero line is the first solid contour).

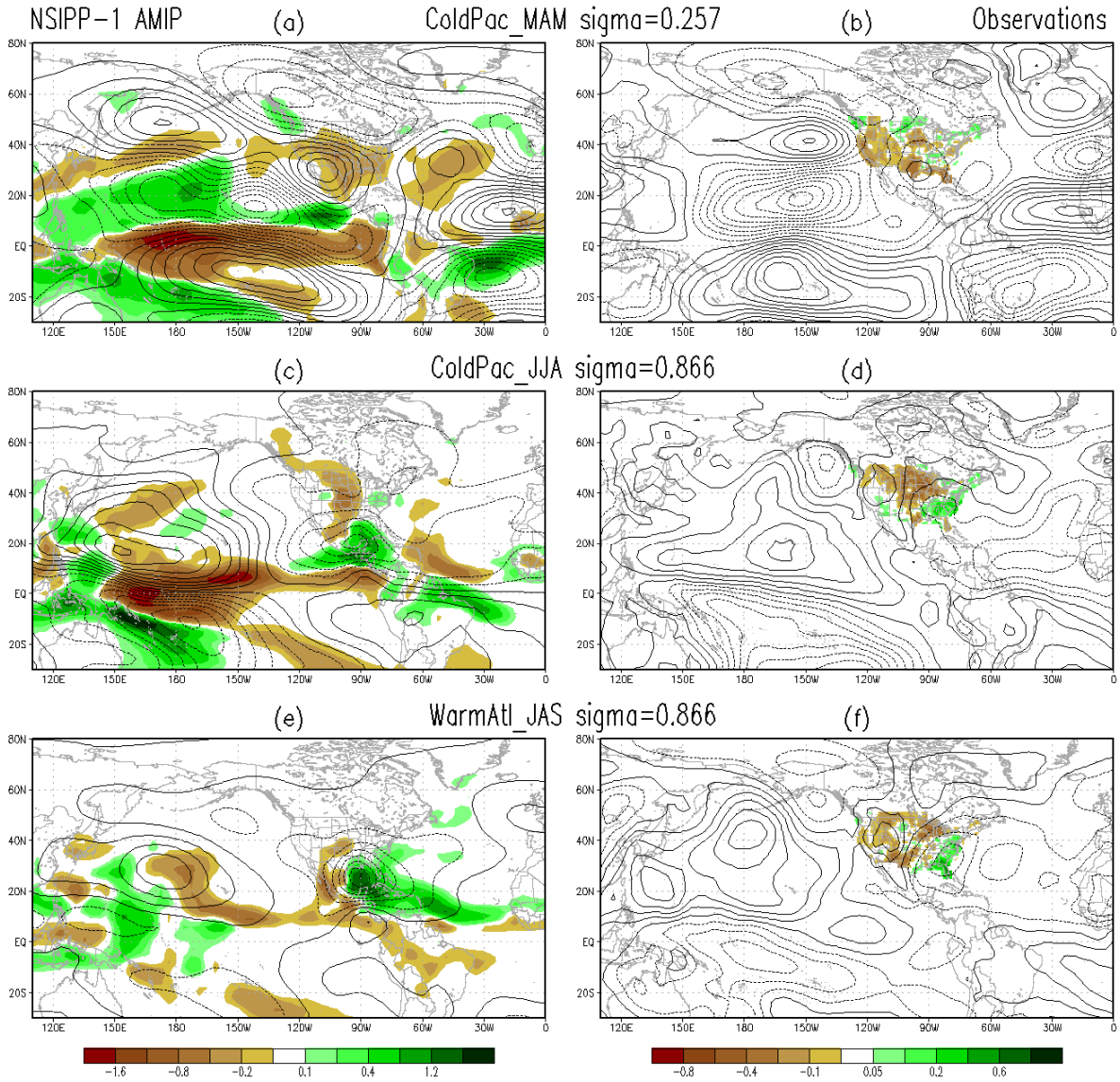


Figure 11. The MAM mean precipitation (mm/day) and eddy streamfunction ( $m^2 s^{-1}$ ) anomalies at $\sigma$ =0.257 associated with the cold Pacific SST pattern in (a) the NSIPP-1 AMIP ensemble mean simulation, and (b) the observations; the precipitation and eddy streamfunction anomalies at $\sigma$ =0.866 associated with the (c) cold Pacific in JJA and (e) warm Atlantic in JAS in the NSIPP-1 AMIP ensemble mean simulation, and associated with the (d) cold Pacific in JJA and (f) warm Atlantic in JAS in the observations. The threshold of 0.5 standard deviation of the PCs of leading SST patterns is used. Note the use of different color scales for the precipitation in the NSIPP AMIP ensemble mean and the observations. Contour intervals of streamfunction are $0.4\times10^6 m^2 s^{-1}$ in (a)-(b) and $0.2\times10^6 m^2 s^{-1}$ in (c)-(f) (negative values are dashed and the zero line is the first solid contour).

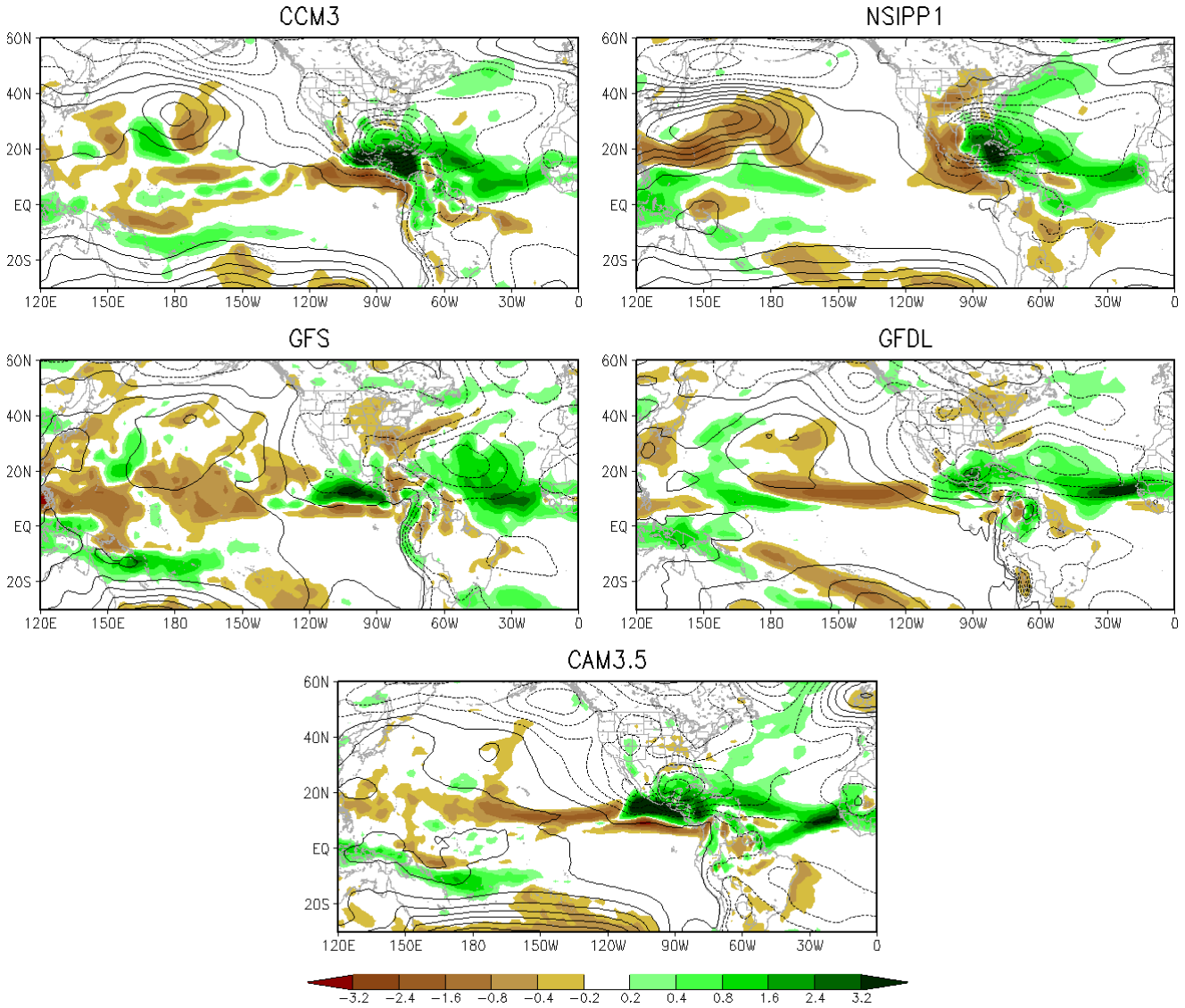


Figure 12. The JAS mean precipitation (mm/day) (shaded) and sea level pressure (millibar) (contour) responses to the warm Atlantic SST pattern in the idealized runs with the five AGCMs. Contour interval of the sea level pressure is 0.3millibar (negative values are dashed and the zero line is the first solid contour).